

Analog Computing for Signal Processing and Communications – Part II: Toward Gigantic MIMO Beamforming

Matteo Nerini, *Member, IEEE*, Bruno Clerckx, *Fellow, IEEE*

Abstract—Analog-domain operations offer a promising solution to accelerating signal processing and enabling future multiple-input multiple-output (MIMO) communications with thousands of antennas. In Part I of this paper, we have introduced a microwave linear analog computer (MiLAC) as an analog computer that processes microwave signals linearly, demonstrating its potential to reduce the computational complexity of specific signal processing tasks. In Part II of this paper, we extend these benefits to wireless communications, showcasing how MiLAC enables gigantic MIMO beamforming entirely in the analog domain. MiLAC-aided beamforming enables the maximum flexibility and performance of digital beamforming, while significantly reducing hardware costs by minimizing the number of radio-frequency (RF) chains and only relying on low-resolution analog-to-digital converters (ADCs) and digital-to-analog converters (DACs). In addition, it eliminates per-symbol operations by completely avoiding digital-domain processing and remarkably reduces the computational complexity of zero-forcing (ZF), which scales quadratically with the number of antennas instead of cubically. It also processes signals with fixed matrices, e.g., the discrete Fourier transform (DFT), directly in the analog domain. Numerical results show that it can perform ZF and DFT with a computational complexity reduction of up to 1.5×10^4 and 4.0×10^7 times, respectively, compared to digital beamforming.

Index Terms—Analog beamforming, analog computing, massive multiple-input multiple-output (MIMO), minimum mean square error (MMSE), zero-forcing (ZF).

I. INTRODUCTION

In Part I of this paper [2], we have reviewed the growing interest in analog computing, driven by advancements in several technologies such as optical systems, metamaterials, and resistive memory arrays. Digital computing, despite its dominance, faces fundamental limitations in speed and power consumption, mainly due to the reliance on analog-to-digital converters (ADCs) and digital-to-analog converters (DACs). Analog computing addresses these challenges by enabling energy-efficient and highly parallelized computations at the speed of light. While Part I has focused on how analog computing can be leveraged for signal processing operations, Part II explores how these principles can be applied to achieve efficient and flexible beamforming in the analog domain, paving the way for future wireless communications.

Part of this work has been accepted by the 2025 IEEE Global Communications Conference (GLOBECOM) [1]. (Corresponding author: Bruno Clerckx.)

This work has been partially supported by UKRI grant EP/Y004086/1, EP/X040569/1, EP/Y037197/1, EP/X04047X/1, and EP/Y037243/1.

Matteo Nerini and Bruno Clerckx are with the Department of Electrical and Electronic Engineering, Imperial College London, London SW7 2AZ, U.K. (e-mail: {m.nerini20, b.clerckx}@imperial.ac.uk).

Bruno Clerckx is also with Kyung Hee University, Seoul, Korea.

As we are witnessing a revival of interest in analog operations within the field of signal processing, a similar shift from digital to analog has emerged in wireless communications. This shift is driven by the growing number of antennas needed to support higher data rates and simultaneously serve a larger number of users. While massive multiple-input multiple-output (MIMO) systems typically deploy 64 or more antennas [3], [4], this number could reach several thousands in ultra-massive or gigantic MIMO systems, which have been recently proposed to meet the stringent requirements of 6G networks [5]. With such a large number of antennas, digital beamforming faces two critical challenges in terms of hardware and computational complexity. First, digital beamforming typically requires a dedicated radio-frequency (RF) chain per antenna element, each including ADCs/DACs and mixers, which are costly and power-hungry components. Second, as the number of antennas increases, the data volumes to be processed in real-time grow accordingly. For example, to precode the transmitted symbol vector at the transmitter (or combine the received symbol vector at the receiver) a matrix-vector product is required on a per-symbol basis. These two challenges result in high hardware costs and computational complexity when digital beamforming is applied in massive or gigantic MIMO systems. For these reasons, several alternatives to digital beamforming have been explored to enable beamforming operations fully or partially in the analog domain.

To address the high hardware cost associated with digital beamforming, alternative strategies such as analog beamforming and hybrid analog-digital beamforming have been proposed. Analog beamforming steers the beam pattern by solely requiring a single RF chain [6]. This is achieved by connecting the RF chain to the antennas via phase shifters or time delay elements, which impose a constant modulus constraint on the beamforming weights. Thus, while analog beamforming offers low hardware complexity, it is characterized by limited flexibility. To balance hardware cost and flexibility by bridging analog and digital beamforming, hybrid analog-digital beamforming techniques have been widely investigated [6], [7], [8], [9], [10], [11]. In hybrid beamforming, the beamforming process is divided into two stages. First, the transmitted symbols are digitally processed in the baseband domain with a low-dimensional digital beamforming matrix, and fed to a reduced number of RF chains. Second, the RF chains are connected to the transmitting antennas through a network of phase shifters, operating analog beamforming in the RF domain. The reversed process is applied at the receiver.

Another method to efficiently perform beamforming in the analog domain is given by reconfigurable intelligent surface (RIS) [12], [13]. This technology has recently emerged enabling the control of the wireless channel through surfaces made of multiple passive elements with reconfigurable scattering properties. Beamforming in the analog domain can be achieved through RIS by deploying a RIS in close proximity to an active transceiving device equipped with a reduced number of antennas. In this way, the effective radiation pattern of the active device can be optimized by reconfiguring the RIS elements [14], [15], [16]. Two extensions of this technology have been proposed to achieve additional flexibility over conventional RIS. First, beyond-diagonal RIS (BD-RIS) include more general RIS architectures, characterized by a scattering matrix not restricted to be diagonal [17], [18], [19]. By deploying a BD-RIS close to an active device, its additional flexibility over conventional RIS in manipulating the radiation pattern can enable even higher performance [20]. Second, stacked intelligent metasurface (SIM) technology considers multiple stacked transmissive RISs deployed close to the active device [21], [22], [23]. The additional flexibility provided by the multiple layers has shown increased performance over just deploying a single conventional RIS. Reconfigurable metasurfaces similar to those in RIS and SIM have been proposed to enable dynamic metasurface antennas (DMAs), and perform beamforming and combining in the analog domain [24], [25], [26].

In the reviewed beamforming strategies operating in the analog domain, the number of RF chains is commonly lower bounded by the number of symbols, or streams, transmitted in parallel. Nevertheless, other beamforming strategies have been developed to also perform symbol modulation in the analog domain, allowing the transmission of multiple symbols with a single RF chain. First, in electronically steerable parasitic array radiators (ESPARs), the symbols are modulated and the radiation pattern reconfigured by adjusting the mutual coupling between one active antenna element and multiple “parasitic” elements having tunable loads [27], [28], [29]. Second, in load modulated arrays (LMAs), a single RF source is connected to multiple antennas through tunable impedance components, which are reconfigured to achieve symbol modulation [30], [31]. Third, symbol modulation can be performed in the analog domain by employing a RIS deployed close to an active antenna transmitting a carrier signal [32], [33]. These three strategies further highlight the potential of leveraging analog-domain beamforming to reduce the hardware cost of transceiver devices.

In addition to alleviating the hardware cost, analog-domain strategies have been also explored to reduce the computational complexity of future wireless networks by performing specific mathematical operations in the analog domain. To this end, in-memory computing has been proposed to accelerate ridge regression with applications to massive MIMO [34], [35], [36]. While in-memory computing approaches can efficiently process baseband signals, other strategies have emerged to directly perform analog processing at RF. RIS and SIM have been used to compute the discrete Fourier transform (DFT) of the incident signal in the analog domain, which is particularly

beneficial for direction-of-arrival (DoA) estimation [37], [38], [39]. Moreover, over-the-air computing emerged as a form of analog computing that leverages the superposition principle characterizing the electromagnetic (EM) propagation over the wireless channels. Over-the-air computing allows efficient computation of the so-called nomographic functions [40], [41], [42], with impactful applications on federated learning [43].

Numerous technologies have been proposed to reduce the hardware cost of future wireless transceivers through analog beamforming [6]-[33] and analog computing [34]-[43]. However, operating in the analog domain typically decreases the flexibility compared to digital beamforming, with a consequent reduction in performance. Thus, whether it is possible to maintain maximum performance while simultaneously minimizing hardware cost and computational complexity through analog computing remains an open question. In Part II of this paper, we address this gap by introducing a novel beamforming strategy enabled by microwave linear analog computers (MiLACs), denoted as MiLAC-aided beamforming. This beamforming strategy maintains the same flexibility as digital beamforming while operating entirely in the analog domain. Because of its fully analog nature, it minimizes the number of RF chains and relies only on low-resolution ADCs/DACs, reducing the hardware cost. By leveraging the computational capabilities of MiLACs, it also minimizes the computational complexity required for beamforming. More in detail, the contributions of Part II of this paper are as follows.

First, we demonstrate that a MiLAC can efficiently process microwave signals to compute five mathematical operations of practical interest in MIMO communications, such as least squares (LS) and matched filtering (MF). To this end, we first show how these five operations can be seen as special cases of the linear minimum mean square error (LMMSE) estimator for linear observation processes, and then discuss how the microwave network of the MiLAC needs to be reconfigured to compute them. These operations can be computed with a MiLAC with significantly reduced computational complexity compared to conventional digital computing.

Second, we propose MiLAC-aided beamforming as a new beamforming strategy enabled by MiLAC scalable to gigantic MIMO systems. MiLAC-aided beamforming can perform precoding at the transmitter and combining at the receiver, directly operating with microwave signals, and maintaining the same flexibility as digital beamforming. While having the maximum flexibility, MiLAC-aided beamforming allows us to perform specific operations in the analog domain, such as zero-forcing (ZF) precoding at the transmitter and ZF combining at the receiver, with important gains in terms of computational complexity. In addition, it allows to precode or combine a signal with a fixed matrix, such as the DFT matrix, entirely in the analog domain, requiring no digital operations.

Third, we compare MiLAC-aided beamforming with existing beamforming strategies, namely digital, analog, hybrid, RIS-aided, and SIM-aided beamforming, in terms of flexibility of the beamforming matrix, hardware complexity, and computational complexity. As a result of this comparison, we discuss five benefits of MiLAC-aided beamforming: 1) it enables the maximum flexibility, 2) it requires the minimum number of

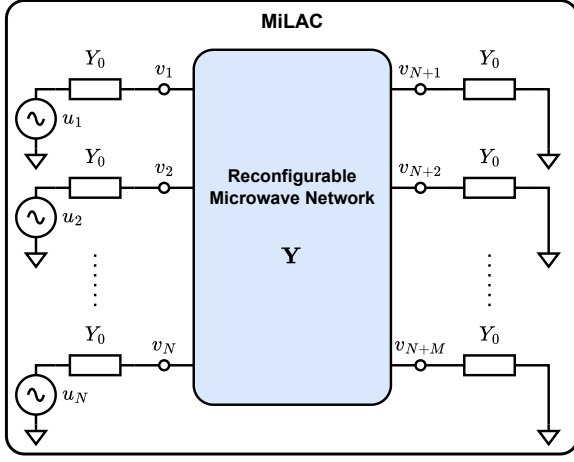


Fig. 1. Representation of a P -port MiLAC with input on N ports, where $P = N + M$.

RF chains, 3) it only needs low-resolution ADCs/DACs, 4) it does not require any computation on a per-symbol basis, and 5) it requires the minimum number of computations per coherence block for ZF.

Fourth, we provide numerical results to assess the performance of MiLAC-aided beamforming in terms of sum rate and bit error rate (BER), confirming that it can achieve the same performance as digital beamforming. We also assess the benefits of MiLAC-aided beamforming over digital beamforming in terms of computational complexity, showing that it can perform ZF, MF, and the DFT with a gain in computational complexity of 1.5×10^4 , 2.0×10^2 , and 4.0×10^7 times, respectively. Thus, in a gigantic MIMO system with thousands of antennas, MiLAC-aided beamforming achieves the same performance as digital ZF beamforming at just 1/15000th of the computational cost. From a different perspective, a 4096-antenna MiLAC serving 4096 users via ZF beamforming requires the same computational complexity as a 256-antenna digital transmitter serving 256 users. This makes MiLAC-aided beamforming a game changer for gigantic MIMO, opening the door to radically new transceiver architectures that can massively scale the number of antennas and users.

Organization: In Section II, we briefly review the concept of MiLAC, as introduced in Part I of this paper. In Section III, we derive five special cases of the LMMSE estimator and show how they can be efficiently computed by a MiLAC. In Section IV, we propose MiLAC-aided beamforming as a novel beamforming strategy enabled by a MiLAC. In Section V, we compare MiLAC-aided beamforming with existing beamforming strategies. In Section VI, we provide numerical results to evaluate the performance and computational complexity of MiLAC-aided beamforming. Finally, Section VII concludes this paper.

Notation: Please, refer to the notation introduced in Section I of Part I of this paper [2].

II. MICROWAVE LINEAR ANALOG COMPUTER

In this section, we briefly review the concept of MiLAC, defined as an analog computer that linearly processes microwave

signals, as introduced in Part I of this paper [2]. A MiLAC can be seen as a P -port reconfigurable microwave network, which can be characterized through its impedance, admittance, or scattering matrix according to multiport network theory. Since these three representations are equivalent, we chose the admittance matrix $\mathbf{Y} \in \mathbb{C}^{P \times P}$ since its entries are closely related to the tunable components in the MiLAC, as seen in Part I. We assume this microwave network to be made of P^2 tunable admittance components interconnecting each port to ground and to all the other ports. The admittance component interconnecting port k to ground is denoted as $Y_{k,k} \in \mathbb{C}$, for $k = 1, \dots, P$, while the admittance component interconnecting port k to port i is denoted as $Y_{i,k} \in \mathbb{C}$, for $\forall i \neq k$. Depending on the admittance values $\{Y_{i,k}\}_{i,k=1}^P$, the entries of the admittance matrix \mathbf{Y} are given by

$$[\mathbf{Y}]_{i,k} = \begin{cases} -Y_{i,k} & i \neq k \\ \sum_{p=1}^P Y_{p,k} & i = k \end{cases}, \quad (1)$$

for $i, k = 1, \dots, P$, as derived in Part I. The relationship in (1) shows that if the P^2 tunable admittance components are arbitrarily reconfigurable, then the admittance matrix \mathbf{Y} can also be arbitrarily reconfigured.

The input signal $\mathbf{u} = [u_1, \dots, u_N]^T \in \mathbb{C}^{N \times 1}$ is applied by N voltage generators with series admittance Y_0 to the first N ports of the MiLAC, with $N \leq P$, as represented in Fig. 1. The output signal is read on all P ports, where $P = N + M$ with M denoting the number of ports with no input, and is denoted by $\mathbf{v} = [v_1, \dots, v_P]^T \in \mathbb{C}^{P \times 1}$, as shown in Fig. 1. For convenience of representation, we introduce the output vectors \mathbf{v}_1 and \mathbf{v}_2 as $\mathbf{v}_1 = [v_1, \dots, v_N]^T \in \mathbb{C}^{N \times 1}$ and $\mathbf{v}_2 = [v_{N+1}, \dots, v_P]^T \in \mathbb{C}^{M \times 1}$, such that $\mathbf{v} = [\mathbf{v}_1^T, \mathbf{v}_2^T]^T$. We consider a MiLAC with $M > 0$ ports with no input in the following.

It has been shown in Part I that the output vectors \mathbf{v}_1 and \mathbf{v}_2 can be expressed as a function of the admittance matrix \mathbf{Y} and the input \mathbf{u} by introducing a matrix $\mathbf{P} \in \mathbb{C}^{P \times P}$ as

$$\mathbf{P} = \frac{\mathbf{Y}}{Y_0} + \mathbf{I}_P, \quad (2)$$

partitioned as

$$\mathbf{P} = \begin{bmatrix} \mathbf{P}_{11} & \mathbf{P}_{12} \\ \mathbf{P}_{21} & \mathbf{P}_{22} \end{bmatrix}, \quad (3)$$

where $\mathbf{P}_{11} \in \mathbb{C}^{N \times N}$, $\mathbf{P}_{12} \in \mathbb{C}^{N \times M}$, $\mathbf{P}_{21} \in \mathbb{C}^{M \times N}$, and $\mathbf{P}_{22} \in \mathbb{C}^{M \times M}$. Assuming \mathbf{P} to be invertible, with \mathbf{P}_{11} or \mathbf{P}_{22} invertible, \mathbf{v}_1 and \mathbf{v}_2 are expressed depending on the invertibility of \mathbf{P}_{11} and \mathbf{P}_{22} as follows:

1) If \mathbf{P}_{11} is invertible, we have

$$\mathbf{v}_1 = \left(\mathbf{P}_{11}^{-1} - \mathbf{P}_{11}^{-1} \mathbf{P}_{12} \right. \\ \left. \times (\mathbf{P}_{21} \mathbf{P}_{11}^{-1} \mathbf{P}_{12} - \mathbf{P}_{22})^{-1} \mathbf{P}_{21} \mathbf{P}_{11}^{-1} \right) \mathbf{u}, \quad (4)$$

$$\mathbf{v}_2 = (\mathbf{P}_{21} \mathbf{P}_{11}^{-1} \mathbf{P}_{12} - \mathbf{P}_{22})^{-1} \mathbf{P}_{21} \mathbf{P}_{11}^{-1} \mathbf{u}. \quad (5)$$

2) If \mathbf{P}_{22} is invertible, we have

$$\mathbf{v}_1 = -(\mathbf{P}_{12} \mathbf{P}_{22}^{-1} \mathbf{P}_{21} - \mathbf{P}_{11})^{-1} \mathbf{u}, \quad (6)$$

$$\mathbf{v}_2 = \mathbf{P}_{22}^{-1} \mathbf{P}_{21} (\mathbf{P}_{12} \mathbf{P}_{22}^{-1} \mathbf{P}_{21} - \mathbf{P}_{11})^{-1} \mathbf{u}. \quad (7)$$

3) If \mathbf{P}_{11} and \mathbf{P}_{22} are both invertible, (4)-(5) and (6)-(7) are equivalent.

Note that (4)-(5) and (6)-(7) express the output vectors \mathbf{v}_1 and \mathbf{v}_2 as a function of the input \mathbf{u} and the blocks of \mathbf{P} , which are directly related to \mathbf{Y} by (2). The expressions (4)-(5) and (6)-(7) can be computed by a MiLAC given any blocks \mathbf{P}_{11} , \mathbf{P}_{12} , \mathbf{P}_{21} , and \mathbf{P}_{22} by setting the tunable admittance components $\{Y_{i,k}\}_{i,k=1}^P$ as a function of any arbitrary \mathbf{P} as

$$Y_{i,k} = \begin{cases} -Y_0 [\mathbf{P}]_{i,k} & i \neq k \\ Y_0 \sum_{p=1}^P [\mathbf{P}]_{p,k} - Y_0 & i = k \end{cases}, \quad (8)$$

for $i, k = 1, \dots, P$, as discussed in Part I. Remarkably, a MiLAC can efficiently compute (4)-(5) and (6)-(7) in the analog domain once the input signals are applied at the input ports, while they would require computationally expensive matrix-matrix products and matrix inversion operations if digitally computed.

III. ANALOG COMPUTING FOR THE SPECIAL CASES OF THE LMMSE ESTIMATOR

In Part I of this paper, we have shown how a MiLAC can be used to compute the LMMSE estimator of a linear observation process with reduced computational complexity. In this section, we derive and discuss five special cases of the LMMSE estimator for linear observation processes, of particular interest in wireless communications. Then, we show how these five special cases can be efficiently computed by a MiLAC.

A. LMMSE Estimator for Linear Observation Processes

Consider a linear observation process $\mathbf{y} = \mathbf{H}\mathbf{x} + \mathbf{n}$, where $\mathbf{y} \in \mathbb{C}^{Y \times 1}$ is the observation vector, $\mathbf{H} \in \mathbb{C}^{Y \times X}$ is a known constant matrix, $\mathbf{x} \in \mathbb{C}^{X \times 1}$ is the unknown random vector with mean $\bar{\mathbf{x}} = \mathbf{0}_{X \times 1}$ and covariance matrix \mathbf{C}_x , and $\mathbf{n} \in \mathbb{C}^{Y \times 1}$ is the random noise vector with mean $\bar{\mathbf{n}} = \mathbf{0}_{Y \times 1}$ and covariance matrix \mathbf{C}_n . We assume that \mathbf{C}_x and \mathbf{C}_n are known and invertible, and that the cross-covariance matrix of \mathbf{x} and \mathbf{n} is $\mathbf{C}_{\mathbf{x}\mathbf{n}} = \mathbf{0}_{X \times Y}$. As discussed in part I, the LMMSE estimator of \mathbf{x} is equivalently given by

$$\hat{\mathbf{x}}_{\text{LMMSE},1} = (\mathbf{H}^H \mathbf{C}_n^{-1} \mathbf{H} + \mathbf{C}_x^{-1})^{-1} \mathbf{H}^H \mathbf{C}_n^{-1} \mathbf{y}, \quad (9)$$

$$\hat{\mathbf{x}}_{\text{LMMSE},2} = \mathbf{C}_x \mathbf{H}^H (\mathbf{H} \mathbf{C}_x \mathbf{H}^H + \mathbf{C}_n)^{-1} \mathbf{y}, \quad (10)$$

where we have $\hat{\mathbf{x}}_{\text{LMMSE},1} = \hat{\mathbf{x}}_{\text{LMMSE},2}$ when $\mathbf{H}^H \mathbf{C}_n^{-1} \mathbf{H} + \mathbf{C}_x^{-1}$ and $\mathbf{H} \mathbf{C}_x \mathbf{H}^H + \mathbf{C}_n$ are both invertible, which holds true in general.

B. Special Cases of the LMMSE Estimator for Linear Observation Processes

The LMMSE estimator in Section III-A has been obtained with no assumptions on the covariance matrices \mathbf{C}_x and \mathbf{C}_n beyond their invertibility. With specific assumptions on \mathbf{C}_x and \mathbf{C}_n , we can show that it includes five special cases of practical interest, as discussed in the following.

TABLE I
SPECIAL CASES OF THE LMMSE ESTIMATOR AND THEIR ASSUMPTIONS.

| Assumptions on \mathbf{C}_x and \mathbf{C}_n | |
|--|---|
| LMMSE | None |
| GLS | $\ \mathbf{C}_x\ _F \gg \ \mathbf{C}_n\ _F$ |
| GMF | $\ \mathbf{C}_x\ _F \ll \ \mathbf{C}_n\ _F$ |
| RLS | $\mathbf{C}_x = \lambda_x \mathbf{I}_X, \mathbf{C}_n = \lambda_n \mathbf{I}_Y$ |
| OLS | $\mathbf{C}_x = \lambda_x \mathbf{I}_X, \mathbf{C}_n = \lambda_n \mathbf{I}_Y, \lambda_x \gg \lambda_n$ |
| OMF | $\mathbf{C}_x = \lambda_x \mathbf{I}_X, \mathbf{C}_n = \lambda_n \mathbf{I}_Y, \lambda_x \ll \lambda_n$ |

1) *Generalized Least Squares*: In generalized least squares (GLS), also known as generalized linear regression, the variance on the a priori information on \mathbf{x} is infinitely higher than on \mathbf{n} , i.e., $\|\mathbf{C}_x\|_F \gg \|\mathbf{C}_n\|_F$. Thus, \mathbf{C}_x^{-1} is negligible in (9) and, equivalently, \mathbf{C}_n is negligible in (10), yielding

$$\hat{\mathbf{x}}_{\text{GLS},1} = (\mathbf{H}^H \mathbf{C}_n^{-1} \mathbf{H})^{-1} \mathbf{H}^H \mathbf{C}_n^{-1} \mathbf{y}, \quad (11)$$

$$\hat{\mathbf{x}}_{\text{GLS},2} = \mathbf{C}_x \mathbf{H}^H (\mathbf{H} \mathbf{C}_x \mathbf{H}^H)^{-1} \mathbf{y}, \quad (12)$$

respectively. Note that, depending on the dimensions of \mathbf{H} , only one matrix among $\mathbf{H}^H \mathbf{C}_n^{-1} \mathbf{H}$ and $\mathbf{H} \mathbf{C}_x \mathbf{H}^H$ may be invertible. Thus, only one among the estimates $\hat{\mathbf{x}}_{\text{GLS},1}$ and $\hat{\mathbf{x}}_{\text{GLS},2}$ may exist.

2) *Generalized Matched Filtering*: Opposite to GLS, we can assume that the variance on the a priori information on \mathbf{x} is infinitely smaller than on \mathbf{n} , i.e., $\|\mathbf{C}_x\|_F \ll \|\mathbf{C}_n\|_F$. In this case, that we denote as generalized matched filtering (GMF), both (9) and (10) boil down to

$$\hat{\mathbf{x}}_{\text{GMF}} = \mathbf{C}_x \mathbf{H}^H \mathbf{C}_n^{-1} \mathbf{y}. \quad (13)$$

3) *Regularized Least Squares*: In regularized least squares (RLS), also known as ridge regression, the entries of \mathbf{x} and \mathbf{n} are uncorrelated and have equal variance, i.e., $\mathbf{C}_x = \lambda_x \mathbf{I}_X$ and $\mathbf{C}_n = \lambda_n \mathbf{I}_Y$, with $\lambda_x, \lambda_n \in \mathbb{R}$ and $\lambda_x, \lambda_n > 0$. Thus, by introducing $\lambda \in \mathbb{R}$ such that $\lambda = \lambda_n / \lambda_x$, (9) and (10) simplify as

$$\hat{\mathbf{x}}_{\text{RLS},1} = (\mathbf{H}^H \mathbf{H} + \lambda \mathbf{I}_X)^{-1} \mathbf{H}^H \mathbf{y}, \quad (14)$$

$$\hat{\mathbf{x}}_{\text{RLS},2} = \mathbf{H}^H (\mathbf{H} \mathbf{H}^H + \lambda \mathbf{I}_Y)^{-1} \mathbf{y}, \quad (15)$$

respectively. Interestingly, the expressions in (14) and (15) are widely used in MIMO wireless communications to realize the so-called regularized zero-forcing beamforming (R-ZFBF) and the minimum mean square error (MMSE) receiver, as effective linear transmission and reception techniques, respectively [44, Chapters 7, 12].

4) *Ordinary Least Squares*: In ordinary least squares (OLS), also simply known as LS, or linear regression, the entries of \mathbf{x} and \mathbf{n} are uncorrelated and have equal variance, i.e., $\mathbf{C}_x = \lambda_x \mathbf{I}_X$ and $\mathbf{C}_n = \lambda_n \mathbf{I}_Y$, and the variance on the a priori information on \mathbf{x} is much higher than on \mathbf{n} , i.e., $\lambda_x \gg \lambda_n$. Thus, since $\lambda = \lambda_n / \lambda_x \ll 1$, (14) and (15) further simplify as

$$\hat{\mathbf{x}}_{\text{OLS},1} = (\mathbf{H}^H \mathbf{H})^{-1} \mathbf{H}^H \mathbf{y}, \quad (16)$$

$$\hat{\mathbf{x}}_{\text{OLS},2} = \mathbf{H}^H (\mathbf{H} \mathbf{H}^H)^{-1} \mathbf{y}, \quad (17)$$

respectively. Interestingly, OLS is a special case of both GLS and RLS as it includes both their assumptions on \mathbf{C}_x and \mathbf{C}_n .

TABLE II
MILAC OUTPUT \mathbf{v}_2 FOR DIFFERENT \mathbf{P} WITH \mathbf{P}_{11} INVERTIBLE.

| | \mathbf{v}_2 | $\begin{bmatrix} \mathbf{P}_{11} & \mathbf{P}_{12} \\ \mathbf{P}_{21} & \mathbf{P}_{22} \end{bmatrix}$ |
|-------|--|---|
| LMMSE | $(\mathbf{H}^H \mathbf{C}_n^{-1} \mathbf{H} + \mathbf{C}_x^{-1})^{-1} \mathbf{H}^H \mathbf{C}_n^{-1} \mathbf{u}$ | $\begin{bmatrix} \pm \mathbf{C}_n & \mathbf{H} \\ \mathbf{H}^H & \mp \mathbf{C}_x^{-1} \end{bmatrix}$ |
| GLS | $(\mathbf{H}^H \mathbf{C}_n^{-1} \mathbf{H})^{-1} \mathbf{H}^H \mathbf{C}_n^{-1} \mathbf{u}$ | $\begin{bmatrix} \pm \mathbf{C}_n & \mathbf{H} \\ \mathbf{H}^H & \mathbf{0}_X \end{bmatrix}$ |
| GMF | $\mathbf{C}_x \mathbf{H}^H \mathbf{C}_n^{-1} \mathbf{u}$ | $\begin{bmatrix} \pm \mathbf{C}_n & \mathbf{0}_{Y \times X} \\ \mathbf{H}^H & \mp \mathbf{C}_x^{-1} \end{bmatrix}$ |
| RLS | $(\mathbf{H}^H \mathbf{H} + \lambda \mathbf{I}_X)^{-1} \mathbf{H}^H \mathbf{u}$ | $\begin{bmatrix} \pm \mathbf{I}_Y & \mathbf{H} \\ \mathbf{H}^H & \mp \lambda \mathbf{I}_X \end{bmatrix}$ |
| OLS | $(\mathbf{H}^H \mathbf{H})^{-1} \mathbf{H}^H \mathbf{u}$ | $\begin{bmatrix} \pm \mathbf{I}_Y & \mathbf{H} \\ \mathbf{H}^H & \mathbf{0}_X \end{bmatrix}$ |
| OMF | $\lambda^{-1} \mathbf{H}^H \mathbf{u}$ | $\begin{bmatrix} \pm \mathbf{I}_Y & \mathbf{0}_{Y \times X} \\ \mathbf{H}^H & \mp \lambda \mathbf{I}_X \end{bmatrix}$ |

As discussed for the GLS, since only one matrix among $\mathbf{H}^H \mathbf{H}$ and $\mathbf{H} \mathbf{H}^H$ may be invertible depending on the dimensions of \mathbf{H} , only one among $\hat{\mathbf{x}}_{\text{OLS},1}$ and $\hat{\mathbf{x}}_{\text{OLS},2}$ may exist, unless \mathbf{H} is a square matrix. Remarkably, the expressions of the OLS are widely employed in MIMO wireless communications to implement zero-forcing beamforming (ZFBE) and the ZF receiver [44, Chapters 7, 12].

5) *Ordinary Matched Filtering*: In ordinary matched filtering (OMF), also simply known as MF, the entries of \mathbf{x} and \mathbf{n} are uncorrelated and have equal variance, i.e., $\mathbf{C}_x = \lambda_x \mathbf{I}_X$ and $\mathbf{C}_n = \lambda_n \mathbf{I}_Y$, and the variance on the a priori information on \mathbf{x} is much smaller than on \mathbf{n} , i.e., $\lambda_x \ll \lambda_n$. Thus, since $\lambda = \lambda_n / \lambda_x \gg 1$, both (14) and (15) boil down to

$$\hat{\mathbf{x}}_{\text{OMF}} = \lambda^{-1} \mathbf{H}^H \mathbf{y}. \quad (18)$$

Remarkably, OMF is a special case of both GMF and RLS as it jointly accounts for their assumptions on \mathbf{C}_x and \mathbf{C}_n . In addition, it is utilized in MIMO wireless communications to realize matched beamforming (MBF) and the MF receiver [44, Chapters 7, 12].

We summarize the five special cases of the LMMSE estimator for linear observation processes and their assumptions on \mathbf{C}_x and \mathbf{C}_n in Tab. I.

C. Computing the Special Cases of the LMMSE Estimator with a MiLAC

The expressions of the five special cases of the LMMSE estimator can be efficiently returned on the output vector \mathbf{v}_2 of a MiLAC having $N = Y$ input ports and $M = X$ output ports with no input, i.e., $P = X + Y$ total ports. This is achieved by exploiting (5) and (7), as discussed for the LMMSE estimator in Part I. First, the tunable admittance components $\{Y_{i,k}\}_{i,k=1}^P$ are set according to (8) such that the blocks of the matrix \mathbf{P} , namely \mathbf{P}_{11} , \mathbf{P}_{12} , \mathbf{P}_{21} , and \mathbf{P}_{22} , give the desired expression in the output \mathbf{v}_2 . Second, the input vector of the MiLAC is set as $\mathbf{u} = \mathbf{y}$. In detail, the expressions of the special cases in (11)-(18) can be computed by setting the blocks of the matrix \mathbf{P} as illustrated in Tabs. II and III, depending on the invertibility of the blocks \mathbf{P}_{11} and \mathbf{P}_{22} . When the block \mathbf{P}_{11} is invertible, \mathbf{v}_2

TABLE III
MILAC OUTPUT \mathbf{v}_2 FOR DIFFERENT \mathbf{P} WITH \mathbf{P}_{22} INVERTIBLE.

| | \mathbf{v}_2 | $\begin{bmatrix} \mathbf{P}_{11} & \mathbf{P}_{12} \\ \mathbf{P}_{21} & \mathbf{P}_{22} \end{bmatrix}$ |
|-------|---|---|
| LMMSE | $\mathbf{C}_x \mathbf{H}^H (\mathbf{H} \mathbf{C}_x \mathbf{H}^H + \mathbf{C}_n)^{-1} \mathbf{u}$ | $\begin{bmatrix} \pm \mathbf{C}_n & \mathbf{H} \\ \mathbf{H}^H & \mp \mathbf{C}_x^{-1} \end{bmatrix}$ |
| GLS | $\mathbf{C}_x \mathbf{H}^H (\mathbf{H} \mathbf{C}_x \mathbf{H}^H)^{-1} \mathbf{u}$ | $\begin{bmatrix} \mathbf{0}_Y & \mathbf{H} \\ \mathbf{H}^H & \mp \mathbf{C}_x^{-1} \end{bmatrix}$ |
| GMF | $\mathbf{C}_x \mathbf{H}^H \mathbf{C}_n^{-1} \mathbf{u}$ | $\begin{bmatrix} \pm \mathbf{C}_n & \mathbf{0}_{Y \times X} \\ \mathbf{H}^H & \mp \mathbf{C}_x^{-1} \end{bmatrix}$ |
| RLS | $\mathbf{H}^H (\mathbf{H} \mathbf{H}^H + \lambda \mathbf{I}_Y)^{-1} \mathbf{u}$ | $\begin{bmatrix} \pm \lambda \mathbf{I}_Y & \mathbf{H} \\ \mathbf{H}^H & \mp \mathbf{I}_X \end{bmatrix}$ |
| OLS | $\mathbf{H}^H (\mathbf{H} \mathbf{H}^H)^{-1} \mathbf{u}$ | $\begin{bmatrix} \mathbf{0}_Y & \mathbf{H} \\ \mathbf{H}^H & \mp \mathbf{I}_X \end{bmatrix}$ |
| OMF | $\lambda^{-1} \mathbf{H}^H \mathbf{u}$ | $\begin{bmatrix} \pm \lambda \mathbf{I}_Y & \mathbf{0}_{Y \times X} \\ \mathbf{H}^H & \mp \mathbf{I}_X \end{bmatrix}$ |

is given by (5), as reported in Tab. II, while when the block \mathbf{P}_{22} is invertible, \mathbf{v}_2 is given by (7), as reported in Tab. III. Note that GLS and OLS are computed via a matrix \mathbf{P} whose blocks \mathbf{P}_{11} and \mathbf{P}_{22} are not both invertible. Thus, for GLS and OLS the expressions in Tabs. II and III are not equivalent in general, while they are equivalent for the LMMSE estimator and the other special cases.

Remark 1. *The five special cases of the LMMSE estimator can be efficiently computed using a MiLAC, which offers significantly reduced computational complexity compared to a digital computer, in terms of the number of arithmetic real operations required. This is because a MiLAC directly performs matrix-matrix multiplications and matrix inversion operations in the analog domain. On the one hand, the computational complexity of computing the special cases with a MiLAC is driven by the number of operations required to compute (8) for a given matrix \mathbf{P} . Thus, the complexity required to compute GLS, RLS, and OLS with a MiLAC is the same as the complexity of computing the LMMSE estimator, i.e., $6XY$ real operations, as discussed in Part I. Besides, computing (8) for the GMF and OMF require approximately $2XY$ real operations for both cases $i \neq k$ and $i = k$, resulting in a total of $4XY$ real operations, where we assumed that the operations involving \mathbf{C}_x and \mathbf{C}_n are precomputed offline. On the other hand, a digital computer calculates the GLS with the same complexity as the LMMSE estimator due to the two matrix-matrix products and matrix inversion, i.e., $8(XY^2 + X^2Y + \min\{X^3, Y^3\}/3)$, as discussed in Part I. The RLS and OLS can be computed with reduced complexity as they require only one matrix-matrix product and a matrix inversion, namely $8 \min\{X^2Y + X^3/3, XY^2 + Y^3/3\}$. Besides, the GMF and OMF only require three and one matrix-vector products, respectively, resulting in a complexity of $8(X^2 + XY + Y^2)$ and $8XY$ real operations, respectively.*

IV. A NOVEL BEAMFORMING STRATEGY:

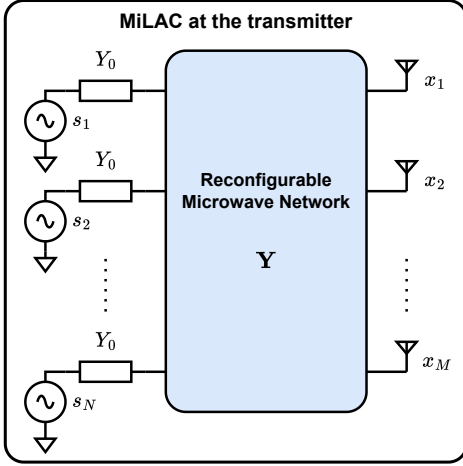


Fig. 2. MiLAC-aided beamforming at the transmitter, performing $\mathbf{x} = \mathbf{W}\mathbf{s}$ in the analog domain, where \mathbf{s} is the symbol vector and \mathbf{W} is an arbitrary precoding matrix.

MiLAC-AIDED BEAMFORMING

In this section, we show how a MiLAC can be used to implement a novel beamforming technique, that we denote as MiLAC-aided beamforming, at the transmitter as well as receiver side. MiLAC-aided beamforming has the same flexibility as digital beamforming, while it offers circuit and computational complexity benefits by fully operating in the analog domain. To illustrate MiLAC-aided beamforming, we consider a MIMO communication system between N_T transmitting antennas and N_R receiving antennas through the wireless channel $\mathbf{H} \in \mathbb{C}^{N_R \times N_T}$. We denote as $\mathbf{x} \in \mathbb{C}^{N_T \times 1}$ the transmitted signal and as $\mathbf{y} \in \mathbb{C}^{N_R \times 1}$ the received signal such that $\mathbf{y} = \mathbf{H}\mathbf{x} + \mathbf{n}$, where $\mathbf{n} \in \mathbb{C}^{N_R \times 1}$ is the additive white Gaussian noise (AWGN)¹. We begin by showing how MiLAC-aided beamforming can be used to implement an arbitrary beamforming matrix.

A. Arbitrary Beamforming

Consider a transmitter that linearly precodes a vector of N_S symbols $\mathbf{s} \in \mathbb{C}^{N_S \times 1}$ to obtain the transmitted signal as $\mathbf{x} = \mathbf{W}\mathbf{s}$, where $\mathbf{W} \in \mathbb{C}^{N_T \times N_S}$ is an arbitrary precoding matrix. Such a transmitter can be implemented purely in the analog domain by a MiLAC having $N = N_S$ ports receiving the symbol vector in input and $M = N_T$ ports delivering the output to antennas perfectly matched to the reference impedance $Z_0 = Y_0^{-1}$, as represented in Fig. 2. Since the antennas are perfectly matched, their Thevenin equivalent circuit is an impedance $Z_0 = Y_0^{-1}$ connected to ground [45, Chapter 2.13]. Thus, the MiLAC in Fig. 2 behaves as when its last N_T ports are connected to ground through an impedance $Z_0 = Y_0^{-1}$, i.e., as analyzed in Section II. Following the analysis in Section II, such a MiLAC returns $\mathbf{x} = \mathbf{W}\mathbf{s}$ on its last N_T ports when the signal \mathbf{s} is fed as input on the first

¹We consider here a general MIMO system, such as single-user MIMO or multi-user with one symbol per user. Both single- and multi-user systems will be specifically studied in the following subsections.

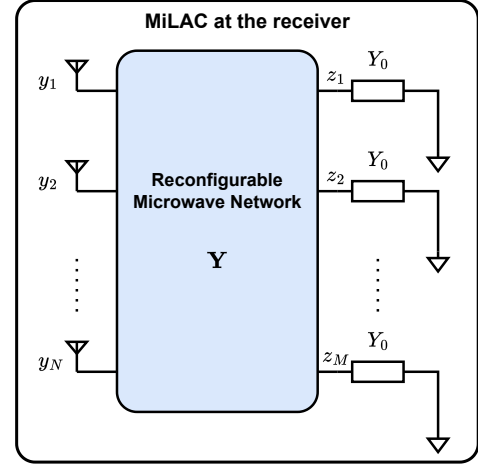


Fig. 3. MiLAC-aided beamforming at the receiver, performing $\mathbf{z} = \mathbf{G}\mathbf{y}$ in the analog domain, where \mathbf{y} is the received signal and \mathbf{G} is an arbitrary combining matrix.

N_S ports and the tunable admittance components are set such that the matrix \mathbf{P} is

$$\mathbf{P} = \begin{bmatrix} \mathbf{I}_{N_S} & \mathbf{0}_{N_S \times N_T} \\ -\mathbf{W} & \mathbf{I}_{N_T} \end{bmatrix}, \quad (19)$$

according to (5) and (7). To this end, the tunable admittance components are set based on (8) where \mathbf{P} is given by (19), yielding

$$Y_{i,k} = \begin{cases} Y_0 [\mathbf{W}]_{i-N,k} & N_S < i, k \leq N_S \\ 0 & \text{Otherwise} \end{cases}, \quad (20)$$

for $i \neq k$, and

$$Y_{k,k} = \begin{cases} -Y_0 \sum_{n_T=1}^{N_T} [\mathbf{W}]_{n_T,k} & k \leq N_S \\ 0 & k > N_S \end{cases}, \quad (21)$$

for $k = 1, \dots, N_S + N_T$. From (20) and (21), we observe that the tunable admittance components of a MiLAC can be reconfigured in closed form to implement any arbitrary beamforming \mathbf{W} matrix in the analog domain. The computational complexity of this beamforming technique, denoted as MiLAC-aided beamforming, is given by the complexity of designing \mathbf{W} (depending on the adopted precoding strategy) and computing (20) and (21) (requiring in total $4N_S N_T$ real operations). Note that these operations are executed at each coherence block, while no operation is required on a per-symbol basis since the matrix-vector product $\mathbf{W}\mathbf{s}$ is performed in the analog domain. To adapt the beamforming matrix \mathbf{W} to the wireless channel \mathbf{H} , the MiLAC is assumed to be implemented with tunable admittance components that can be reconfigured at every channel coherence time.

As discussed on the transmitter side, MiLAC-aided beamforming can also be introduced on the receiver side. Specifically, a MiLAC can be used to linearly combine the received signal $\mathbf{y} \in \mathbb{C}^{N_R \times 1}$ to obtain the signal used for detection $\mathbf{z} \in \mathbb{C}^{N_S \times 1}$ as $\mathbf{z} = \mathbf{G}\mathbf{y}$, where $\mathbf{G} \in \mathbb{C}^{N_S \times N_R}$ is an arbitrary combining matrix. This can be obtained with MiLAC having $N = N_R$ ports acquiring the input from the receiving antennas and $M = N_S$ ports providing the output vector \mathbf{z} ,

as represented in Fig. 3. Note that in Fig. 3 we assume the antennas to be perfectly matched to the reference impedance $Z_0 = Y_0^{-1}$, such that their Thevenin equivalent circuit is a voltage generator (inducing a voltage y_n at port n , for $n = 1, \dots, N$) in series to an impedance $Z_0 = Y_0^{-1}$ [45, Chapter 2.13], i.e., as in the MiLAC analyzed in Section II.

Among the possible linear precoding and combining strategies, MiLAC-aided beamforming can efficiently perform R-ZFBF, ZFBF, and MBF at the transmitter and MMSE, ZF, and MF at the receiver by exploiting the capability of a MiLAC to compute the corresponding special case of the LMMSE estimator. This leads to remarkable computational complexity benefits, as illustrated in the following.

B. LMMSE-Inspired Beamforming at the Transmitter: R-ZFBF, ZFBF, and MBF Transmitters

Assume that the previously considered MIMO system $\mathbf{y} = \mathbf{H}\mathbf{x} + \mathbf{n}$ is a multi-user system between an N_T -antenna transmitter and N_R single-antenna users, with $N_R \leq N_T$. The signal received at the N_R users \mathbf{y} is used to detect the symbols $\mathbf{s} \in \mathbb{C}^{N_S \times 1}$, with $N_S = N_R$, and the transmitted signal is given by $\mathbf{x} = \mathbf{W}\mathbf{s}$, where $\mathbf{W} \in \mathbb{C}^{N_T \times N_R}$ is the precoding matrix implemented by a MiLAC, as in Fig. 2. By exploiting the operations included in Tab. III, it is possible to reconfigure the microwave network of the MiLAC to efficiently execute three popular linear transmitters [44, Chapter 12]. First, a MiLAC computing RLS can realize R-ZFBF, with precoding matrix $\mathbf{W}_{\text{R-ZFBF}} = \mathbf{H}^H(\mathbf{H}\mathbf{H}^H + \lambda\mathbf{I}_{N_R})^{-1}$, where λ is an arbitrary regularization factor. Second, ZFBF can be implemented by a MiLAC computing OLS, whose precoding matrix is $\mathbf{W}_{\text{ZFBF}} = \mathbf{H}^H(\mathbf{H}\mathbf{H}^H)^{-1}$. Third, a MiLAC computing OMF can realize MBF, with precoding matrix given by $\mathbf{W}_{\text{MBF}} = \lambda^{-1}\mathbf{H}^H$. These three transmitters are obtained by reconfiguring the tunable admittance components of the MiLAC according to the channel \mathbf{H} on a per coherence block basis, and do not require any operation on a per-symbol basis. In addition, they require ultra-low computational complexity on a per coherence block basis since the matrix \mathbf{P} of the MiLAC is readily given as a function of the wireless channel \mathbf{H} . Hence, the only operations required are to compute the admittance values $\{Y_{i,k}\}_{i,k=1}^P$ from \mathbf{P} .

Remark 2. According to Remark 1, the R-ZFBF and ZFBF transmitters can be achieved with only $6N_T N_R$ real operations, while the MBF transmitter with only $4N_T N_R$ real operations, which are necessary to set the tunable admittance components of the MiLAC. Conversely, the computational complexity of digitally calculating the R-ZFBF and ZFBF transmitters is $8(N_T N_R^2 + N_R^3/3)$ real operations, while for the MBF transmitter is $8N_T N_R$. This confirms the significant benefits of MiLAC-aided beamforming in terms of computational complexity, especially in implementing the R-ZFBF and ZFBF transmitters.

C. LMMSE-Inspired Beamforming at the Receiver: MMSE, ZF, and MF Receivers

Assume that the MIMO system $\mathbf{y} = \mathbf{H}\mathbf{x} + \mathbf{n}$ is a single-user system between an N_T -antenna transmitter and a N_R -

antenna receiver, with $N_R \geq N_T$. The transmitted signal \mathbf{x} contains the symbols to be detected at the receiver, i.e., $\mathbf{x} = \mathbf{s}$, and the receiver uses the signal $\mathbf{z} = \mathbf{G}\mathbf{y} \in \mathbb{C}^{N_T \times 1}$ to accurately detect the symbols, where $\mathbf{G} \in \mathbb{C}^{N_T \times N_R}$ is the combining matrix imposed by the MiLAC, as in Fig. 3. By using the operations in Tab. II, it is possible to reconfigure the microwave network of the MiLAC to efficiently implement three widely used receivers [44, Chapter 7]. First, a MiLAC computing RLS can realize the MMSE receiver with combining matrix $\mathbf{G}_{\text{MMSE}} = (\mathbf{H}^H \mathbf{H} + \lambda \mathbf{I}_{N_T})^{-1} \mathbf{H}^H$. If the covariance matrix of the transmitted signal \mathbf{x} is $\mathbf{C}_x = P_T/N_T \mathbf{I}_{N_T}$, where P_T is the transmit power, and the covariance matrix of the noise \mathbf{n} is $\mathbf{C}_n = \sigma_n^2 \mathbf{I}_{N_R}$, where σ_n^2 is the noise power, the optimal regularization factor λ is given by $\lambda = N_T \sigma_n^2 / P_T$ [44, Chapter 7]. Second, the ZF receiver can be realized by a MiLAC computing OLS, whose combining matrix is $\mathbf{G}_{\text{ZF}} = (\mathbf{H}^H \mathbf{H})^{-1} \mathbf{H}^H$. Third, a MiLAC computing OMF can implement the MF receiver, with combining matrix $\mathbf{G}_{\text{MF}} = \lambda^{-1} \mathbf{H}^H$, where the optimal λ is $\lambda = N_T \sigma_n^2 / P_T$ if $\mathbf{C}_x = P_T/N_T \mathbf{I}_{N_T}$ and $\mathbf{C}_n = \sigma_n^2 \mathbf{I}_{N_R}$ [44, Chapter 7]. These three receivers are realized by solely reconfiguring the MiLAC on a per coherence block basis, while no operation is required on a per-symbol basis.

Remark 3. Similarly to Remark 2, the MMSE and ZF receivers can be obtained through a MiLAC with only $6N_T N_R$ real operations and the MF receiver with only $4N_T N_R$ real operations, which are required to set the tunable admittance components. In contrast, the computational complexity of digitally calculating the MMSE and ZF receivers is $8(N_T^2 N_R + N_T^3/3)$ real operations, and for the MF receiver is $8N_T N_R$, showing important benefits in using MiLAC-aided beamforming to implement the MMSE and ZF receivers.

D. Computing the DFT

MiLAC-aided beamforming is also beneficial when used to precode or combine a signal with a fixed beamforming matrix. In this case, since the admittance components of the MiLAC are optimized offline, no operation is required online with MiLAC-aided beamforming, while a matrix-vector product is needed on a per-symbol basis in the case of digital beamforming. Combining the received signal \mathbf{y} with a fixed matrix \mathbf{G} is particularly useful for DoA estimation, where the received signal is typically multiplied by the DFT matrix [39]. This operation performed at the receiver can be formalized as $\mathbf{z} = \mathbf{G}\mathbf{y}$, where $\mathbf{G} \in \mathbb{C}^{N_R \times N_R}$ is the DFT matrix, given by

$$[\mathbf{G}]_{i,k} = \frac{1}{\sqrt{N_R}} e^{-j2\pi \frac{(i-1)(k-1)}{N_R}}, \quad (22)$$

for $i, k = 1, \dots, N_R$. This operation can be implemented purely in the analog domain by a MiLAC having $N = N_R$ ports acquiring the input \mathbf{y} from the receiving antennas and $M = N_R$ ports returning the output, as represented in Fig. 3. To perform such a DFT operation, the admittance components of the MiLAC need to be set offline following (8) where the matrix \mathbf{P} given by

$$\mathbf{P} = \begin{bmatrix} \mathbf{I}_{N_R} & \mathbf{0}_{N_R \times N_R} \\ -\mathbf{G} & \mathbf{I}_{N_R} \end{bmatrix}, \quad (23)$$

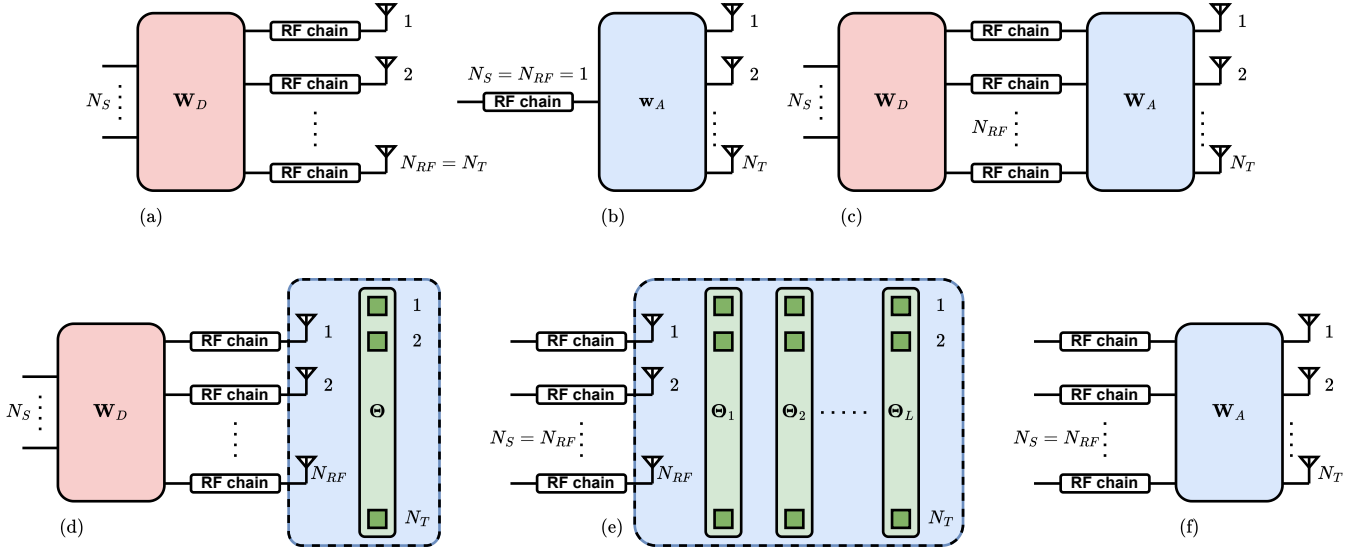


Fig. 4. (a) Digital, (b) analog, (c) hybrid, (d) RIS-aided, (e) SIM-aided, and (f) MiLAC-aided beamforming at the transmitter.

TABLE IV
BEAMFORMING STRATEGIES COMPARISON.

| Beamforming | Precoding matrix | Constraints | Number of RF chains | Resolution of ADCs/DACs | Operations per symbol basis | Operations per coherence block |
|-------------|---|---|---------------------|-------------------------|-----------------------------------|---------------------------------------|
| Digital | \mathbf{W}_D | $\mathbf{W}_D \in \mathbb{C}^{N_T \times N_S}$ | $N_{RF} = N_T$ | High | Compute $\mathbf{W}_D \mathbf{s}$ | Optimize \mathbf{W}_D |
| Analog | \mathbf{w}_A | $\mathbf{w}_A \in \mathbb{T}^{N_T \times 1}$ | $N_{RF} = N_S = 1$ | Low | None | Optimize \mathbf{w}_A |
| Hybrid | $\mathbf{W}_A \mathbf{W}_D$ | $\mathbf{W}_D \in \mathbb{C}^{N_{RF} \times N_S}$ $\mathbf{W}_A \in \mathbb{T}^{N_T \times N_{RF}}$ | $N_{RF} \geq N_S$ | High | Compute $\mathbf{W}_D \mathbf{s}$ | Optimize $\mathbf{W}_D, \mathbf{W}_A$ |
| RIS-aided | $\Theta \mathbf{H}_{\text{RIS}} \mathbf{W}_D$ | $\mathbf{W}_D \in \mathbb{C}^{N_{RF} \times N_S}$ $\mathbf{H}_{\text{RIS}} \in \mathbb{C}^{N_T \times N_{RF}}$, fixed $\Theta \in \mathbb{C}^{N_T \times N_T}$, $\Theta^H \Theta = \mathbf{I}_{N_T}$ | $N_{RF} \geq N_S$ | High | Compute $\mathbf{W}_D \mathbf{s}$ | Optimize \mathbf{W}_D, Θ |
| SIM-aided | $\Theta_L \mathbf{H}_{\text{SIM},L} \cdots \cdots \Theta_1 \mathbf{H}_{\text{SIM},1}$ | $\mathbf{H}_{\text{SIM},1} \in \mathbb{C}^{N_T \times N_{RF}}$, fixed $\mathbf{H}_{\text{SIM},\ell} \in \mathbb{C}^{N_T \times N_T}$, $\ell > 2$, fixed $\Theta_\ell \in \mathbb{C}^{N_T \times N_T}$, $\Theta_\ell^H \Theta_\ell = \mathbf{I}_{N_T}$ | $N_{RF} = N_S$ | Low | None | Optimize Θ_ℓ |
| MiLAC-aided | \mathbf{W}_A | $\mathbf{W}_A \in \mathbb{C}^{N_T \times N_S}$ | $N_{RF} = N_S$ | Low | None | Optimize $Y_{i,k}$ |

with \mathbf{G} being the DFT matrix in (22). Thus, by substituting (22) and (23) into (8), we obtain that the admittance components $\{Y_{i,k}\}_{i,k=1}^{2N_R}$ are set as

$$Y_{i,k} = \begin{cases} \frac{Y_0}{\sqrt{N_R}} e^{-j2\pi \frac{(i-N-1)(k-1)}{N_R}} & N_R < i, k \leq N_R \\ 0 & \text{Otherwise} \end{cases}, \quad (24)$$

for $i \neq k$, and

$$Y_{k,k} = \begin{cases} -Y_0 \sqrt{N_R} & k = 1 \\ 0 & k \neq 1 \end{cases}, \quad (25)$$

for $k = 1, \dots, 2N_R$.

Remark 4. By employing a MiLAC with fixed admittance components set as in (24) and (25), we can perform the DFT instantly in the analog domain requiring no digital operations. Conversely, the DFT requires approximately $34/9 N_R \log_2(N_R)$ real operations to be digitally computed [46], which could become prohibitive as the number of antennas N_R grows extremely large. Note that we assume a one-dimensional DFT for simplicity, while a similar discussion

also holds to perform a two-dimensional DFT in the analog domain, as considered in [39].

V. COMPARISON WITH EXISTING BEAMFORMING STRATEGIES

We have discussed how a MiLAC can enable MiLAC-aided beamforming, a new beamforming strategy purely in the analog domain having the same flexibility as digital beamforming. In this section, we highlight the benefits of MiLAC-aided beamforming over the state-of-the-art beamforming strategies, showing that it requires fewer RF chains, lower-resolution ADCs/DACs, and reduced computational complexity. To this end, we consider a transmitter with N_T antennas and N_{RF} RF chains transmitting N_S symbols, where we have $N_S \leq N_{RF} \leq N_T$. We denote as $\mathbf{s} \in \mathbb{C}^{N_S \times 1}$ the symbol vector

²Several strategies have been proposed to perform symbol modulation in the analog domain, i.e., through ESPAR [27], [28], [29], LMA [30], [31], and RIS [32], [33], which can enable multi-stream transmissions ($N_S > 1$) with $N_{RF} = 1$ RF chain. However, these strategies operate symbol modulation on a per-symbol basis, and are fundamentally different from beamforming strategies acting per coherence block.

and as $\mathbf{x} \in \mathbb{C}^{N_T \times 1}$ the transmitted signal. The following discussion for a transmitter readily applies also for a receiver.

A. Digital Beamforming

In digital beamforming, the transmitted signal is given by $\mathbf{x} = \mathbf{W}_D \mathbf{s}$, where $\mathbf{W}_D \in \mathbb{C}^{N_T \times N_S}$ is the digital precoder, subject only to the power constraint. To allow maximum flexibility, there are $N_{RF} = N_T$ RF chains equipped high-resolution ADCs/DACs, each carrying an entry of the transmitted signal \mathbf{x} to the corresponding antenna, as in Fig. 4(a). In addition, the computational complexity is driven by the matrix-vector product $\mathbf{W}_D \mathbf{s}$ executed on a per-symbol basis and by the optimization of \mathbf{W}_D at each coherence block based on the channel realization, whose complexity depends on the specific digital precoding strategy.

B. Analog Beamforming

In analog beamforming [6], only one symbol $s \in \mathbb{C}$ is transmitted ($N_S = 1$), and the transmitted signal is given by $\mathbf{x} = \mathbf{w}_A s$, where $\mathbf{w}_A \in \mathbb{C}^{N_T \times 1}$ is the analog precoder, as in Fig. 4(b). Since the symbol s reaches the N_T antennas by passing through N_T phase shifters, the analog precoder is subject to $\mathbf{w}_A \in \mathbb{T}^{N_T \times 1}$, where $\mathbb{T} = \{c \in \mathbb{C} : |c| = 1\}$, due to the unit-modulus constraint imposed by the phase shifters. In this case, a single RF chain is sufficient to carry the symbol s , which can be equipped with low-resolution ADCs/DACs since the symbol s lies in a constellation with finite cardinality. The computational complexity of analog beamforming is given by the complexity of optimizing \mathbf{w}_A at every coherence block as a function of the channel realization. Note that no operation takes place on a per-symbol basis since the product $\mathbf{w}_A s$ is performed in the analog domain as the signal flows through the phase shifters connected to all antennas.

C. Hybrid Beamforming

In hybrid beamforming [6], [7], [8], [9], [10], the transmitted signal is $\mathbf{x} = \mathbf{W}_A \mathbf{W}_D \mathbf{s}$, where $\mathbf{W}_A \in \mathbb{C}^{N_T \times N_{RF}}$ is the analog precoder, subject to specific constraints depending on the architecture of phase shifters and switches, and $\mathbf{W}_D \in \mathbb{C}^{N_{RF} \times N_S}$ is the digital precoder, subject only to the power constraint, as in Fig. 4(c). Thus, the effective precoding matrix is given by $\mathbf{W} = \mathbf{W}_A \mathbf{W}_D$. Numerous hybrid beamforming architectures have been proposed, each with different constraints on the matrix \mathbf{W}_A . For example, in the fully-connected architecture, each RF chain is connected to all the antennas through a phase shifter, and each entry of \mathbf{W}_A is subject to the unit-modulus constraint, i.e., $\mathbf{W}_A \in \mathbb{T}^{N_T \times N_{RF}}$. The computational complexity of hybrid beamforming is given by the complexity of computing the matrix-vector product $\mathbf{W}_D \mathbf{s}$ on a per-symbol basis, and optimizing \mathbf{W}_A and \mathbf{W}_D at each coherence block. This is because the digitally precoded signal $\mathbf{W}_D \mathbf{s}$ is multiplied by \mathbf{W}_A in the analog domain. Although the network of phase shifters in hybrid beamforming can operate a matrix-vector product in the analog domain, it cannot compute non-linear operations as a MiLAC made of admittance components.

D. RIS-Aided Beamforming

As a related analog-domain beamforming strategy, RIS-aided beamforming emerged by exploiting a RIS deployed in close proximity with an active transmitting device [14], [15], [16], [20], as in Fig. 4(d). The RIS can work in either reflective or transmissive mode, without changing the system model. Denoting as $\mathbf{x}' = \mathbf{W}_D \mathbf{s}$ the digitally precoded signal transmitted by the active device, the received signal is given by $\mathbf{y} = \mathbf{H}_{\text{EFF}} \mathbf{x}'$, where $\mathbf{H}_{\text{EFF}} \in \mathbb{C}^{N_R \times N_{RF}}$ is the RIS-aided channel, given by $\mathbf{H}_{\text{EFF}} = \mathbf{H} \mathbf{\Theta} \mathbf{H}_{\text{RIS}}$, with $\mathbf{H} \in \mathbb{C}^{N_R \times N_T}$, $\mathbf{\Theta} \in \mathbb{C}^{N_T \times N_T}$, and $\mathbf{H}_{\text{RIS}} \in \mathbb{C}^{N_T \times N_{RF}}$ being the channel from the RIS to the receiver, the scattering matrix of the RIS, and the channel from the active transmitting device to the RIS, respectively. Thus, effective precoding matrix is $\mathbf{W} = \mathbf{\Theta} \mathbf{H}_{\text{RIS}} \mathbf{W}_D$, which is optimized by reconfiguring $\mathbf{\Theta}$, subject to $\mathbf{\Theta}^H \mathbf{\Theta} = \mathbf{I}_{N_T}$ in the case of an ideal lossless RIS [17], \mathbf{H}_{RIS} is not reconfigurable, and \mathbf{W}_D , subject only to the power constraint. As in hybrid beamforming, the matrix-vector product $\mathbf{W}_D \mathbf{s}$ needs to be computed on a per-symbol basis, while \mathbf{W}_D and $\mathbf{\Theta}$ are optimized per coherence block.

E. SIM-Aided Beamforming

RIS-aided beamforming has been extended by stacking multiple transmissive RISs at the transmitter, which is denoted in the literature as a SIM [21], [22], [23], as in Fig. 4(e). Given the additional flexibility provided by the multiple metasurfaces, SIM-aided beamforming does not include any digital precoding, and for this reason it only requires $N_{RF} = N_S$ RF chains equipped with low-resolution ADCs/DACs [21], [22], [23], [39]. Similar to RIS-aided beamforming, SIM-aided beamforming exploits the fact that the effective channel between the transmitter and receiver can be engineered by reconfiguring the scattering matrices of the stacked RISs. Assuming a SIM made of L stacked RISs each with N_T elements, the effective channel between the active device transmitting the symbols \mathbf{s} and the receiver is given by

$$\mathbf{H}_{\text{EFF}} = \mathbf{H} \mathbf{\Theta}_L \mathbf{H}_{\text{SIM},L} \cdots \mathbf{\Theta}_2 \mathbf{H}_{\text{SIM},2} \mathbf{\Theta}_1 \mathbf{H}_{\text{SIM},1}, \quad (26)$$

where $\mathbf{H} \in \mathbb{C}^{N_R \times N_T}$, $\mathbf{\Theta}_\ell \in \mathbb{C}^{N_T \times N_T}$, and $\mathbf{H}_{\text{SIM},\ell} \in \mathbb{C}^{N_T \times N_T}$ are the channel from the L th RIS to the receiver, the scattering matrix of the ℓ th RIS, and the channel from the $\ell - 1$ th to the ℓ th RIS (where the 0th RIS is the transmitting device and $\mathbf{H}_{\text{SIM},1} \in \mathbb{C}^{N_T \times N_{RF}}$), respectively. Thus, the effective precoding matrix reads as

$$\mathbf{W} = \mathbf{\Theta}_L \mathbf{H}_{\text{SIM},L} \cdots \mathbf{\Theta}_2 \mathbf{H}_{\text{SIM},2} \mathbf{\Theta}_1 \mathbf{H}_{\text{SIM},1}, \quad (27)$$

which is optimized per coherence block by reconfiguring the scattering matrices of the L stacked RISs $\mathbf{\Theta}_\ell$, for $\ell = 1, \dots, L$.

Since SIM-aided beamforming is entirely performed in the analog domain, it can be regarded as a low-complexity approach for implementing MiLAC-aided beamforming, with fewer tunable admittance components. Due to the reduced number of tunable components, the flexibility of the beamforming matrix is consequently reduced, and it is constrained as in (27) and cannot be an arbitrary matrix.

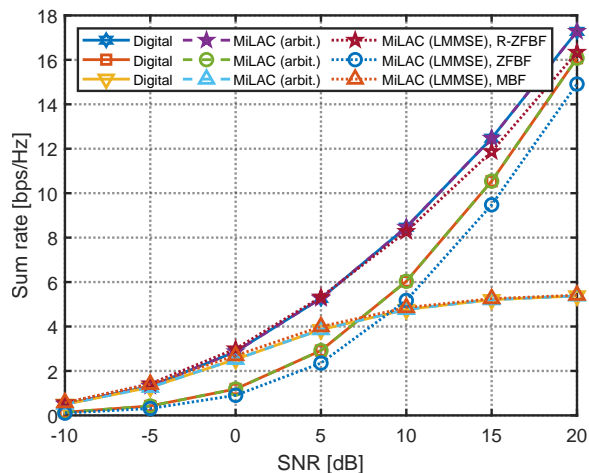


Fig. 5. Sum rate in a 4×4 multi-user MISO system, with digital and MiLAC-aided beamforming at the transmitter.

F. MiLAC-Aided Beamforming

In MiLAC-aided beamforming, the symbols \mathbf{s} are given in input to a MiLAC, and the transmitted signal \mathbf{x} is returned on its output ports, as explained in Section IV. This novel beamforming strategy brings five unique benefits over state-of-the-art beamforming strategies. Specifically, it offers the maximum flexibility with minimum hardware complexity (in terms of the number of RF chains and resolution of ADCs/DACs) and minimum computational complexity (in terms of operations per-symbol basis and per coherence block).

1) *Maximum Flexibility*: MiLAC-aided beamforming has the same flexibility as digital beamforming since it can apply any arbitrary beamforming matrix \mathbf{W} , as illustrated in Section IV. Given its full flexibility, MiLAC-aided beamforming can obtain the same performance as digital beamforming, outperforming other beamforming strategies that impose limiting constraints on \mathbf{W} , i.e., analog, hybrid, RIS-aided, and SIM-aided, as summarized in Tab. IV.

2) *Minimum Number of RF Chains*: In MiLAC-aided beamforming, the symbols are fed in input to the MiLAC, which computes the transmitted signal in the analog domain. Thus, only $N_{RF} = N_S$ RF chains are needed to achieve the full flexibility of digital beamforming, which is the minimum number of RF chains requested by the reviewed beamforming strategies, as shown in Tab. IV. Note that a fully-connected hybrid beamforming architecture requires $N_{RF} = 2N_S$ RF chains to realize any digital beamforming matrix [8], while the other beamforming strategies are not proven to achieve full flexibility with any $N_{RF} < N_T$.

3) *Low-resolution ADCs/DACs*: Since MiLAC-aided beamforming processes the symbols purely in the analog domain, each RF chain carries an individual symbol, which lies in a constellation with finite cardinality. For example, in the case of quadrature phase shift keying (QPSK), the symbols can be chosen from the constellation $\{+1+j, +1-j, -1-j, -1+j\}$, up to a scaling factor, which can be generated through DACs having just 1-bit resolution for both in-phase and quadrature parts of the signal. Thus, low-resolution ADCs/DACs can be adopted without sacrificing performance, which are

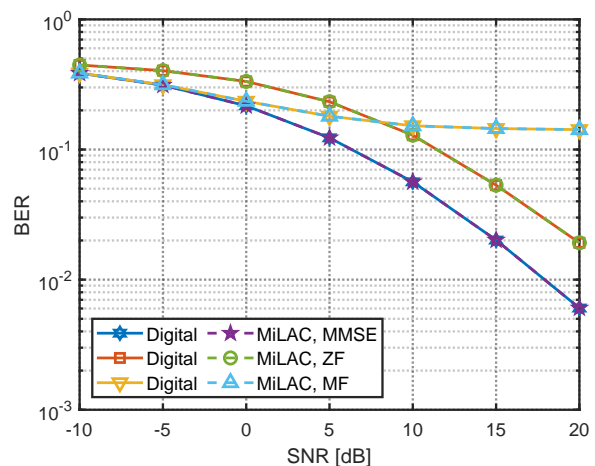


Fig. 6. BER in a 4×4 single-user MIMO system using QPSK, with digital and MiLAC-aided beamforming at the receiver.

less expensive and less power-hungry than high-resolution ADCs/DACs. High-resolution ADCs/DACs are instead necessary when beamforming is performed in the digital domain (entirely or in part), i.e., in digital beamforming, hybrid beamforming, and RIS-aided beamforming, as indicated in Tab. IV.

4) *No Computations on a Per-Symbol Basis*: If beamforming is performed in the digital domain (entirely or in part), the matrix-vector product $\mathbf{W}_D \mathbf{s}$ needs to be computed on a per-symbol basis, as shown in Tab. IV. The complexity of this operation is $8N_{RF}N_S$ real operations, as discussed in the Appendix of Part I, and can become prohibitive in massive/gigantic MIMO systems [4]. MiLAC-aided beamforming solves this issue since it does not require any computation on a per-symbol basis, as the beamforming is purely analog. This reduces the beamforming computational complexity, especially when the coherence time is much longer than the symbol time [4].

5) *Minimum Computations Per Coherence Block for RLS and OLS*: MiLAC-aided beamforming offers further gains in terms of computational complexity by exploiting the capability of a MiLAC to efficiently compute RLS and OLS in the analog domain. Specifically, these gains can be obtained when MiLAC-aided beamforming is used to compute the R-ZFBF and ZFBF transmitters or the MMSE and ZF receivers, as discussed in Section IV.

VI. NUMERICAL RESULTS

We have proposed MiLAC-aided beamforming as a novel beamforming strategy that offers the same flexibility as digital beamforming, while presenting promising advantages in terms of circuit and computational complexity. In this section, we evaluate the performance and computational complexity of MiLAC-aided beamforming.

A. Performance Evaluation

Since MiLAC-aided beamforming can implement any arbitrary beamforming matrix, it is proven to perform as digital

beamforming and outperform other beamforming strategies that are limited by constrained beamforming matrices. The specific performance gains over the reviewed beamforming strategies match those of digital beamforming, which depend on the performance metric and scenario, such as whether the transmission is single- or multi-stream, and whether the system is single- or multi-user. Thus, we analyze the cases where MiLAC-aided beamforming leverages the computing capabilities of a MiLAC to implement the LMMSE-inspired beamforming matrices, i.e., R-ZFBF, ZFBF, and MBF at the transmitter, and the MMSE, ZF, and MF at the receiver.

To evaluate the performance of R-ZFBF, ZFBF, and MBF realized with digital and MiLAC-aided beamforming, we consider a multi-user multiple-input single-output (MISO) system with an N_T -antenna transmitter and N_R single-antenna receivers, as presented in Section IV-B. Here, the transmitter precodes the N_R symbols $\mathbf{s} \in \mathbb{C}^{N_R \times 1}$ intended to the N_R receivers through R-ZFBF or ZFBF to suppress inter-stream interference, or through MBF to maximize the channel gains. With digital beamforming, the R-ZFBF transmitter is realized by computing $\mathbf{F}_{\text{R-ZFBF}} = \mathbf{H}^H (\mathbf{H}\mathbf{H}^H + \lambda \mathbf{I}_{N_R})^{-1}$ and setting the precoding matrix $\mathbf{W}_{\text{R-ZFBF}}$ such that $[\mathbf{W}_{\text{R-ZFBF}}]_{:,n_R} = [\mathbf{F}_{\text{R-ZFBF}}]_{:,n_R} / \|\mathbf{F}_{\text{R-ZFBF}}\|_2$, for $n_R = 1, \dots, N_R$, assuming uniform power allocation to the users. For large N_R and if the signal-to-noise ratio (SNR) is the same at all receiving antennas, the optimal λ is $\lambda = N_R \sigma_n^2 / P_T$, where P_T is the transmit power, i.e., \mathbf{s} has covariance matrix $\mathbf{C}_s = P_T / N_R \mathbf{I}_{N_R}$, σ_n^2 is the noise power, and we assumed the channel to have unit path gain [44, Chapter 12]. Similarly, digital beamforming can realize ZFBF by computing $\mathbf{F}_{\text{ZFBF}} = \mathbf{H}^H (\mathbf{H}\mathbf{H}^H)^{-1}$ and setting \mathbf{W}_{ZFBF} as $[\mathbf{W}_{\text{ZFBF}}]_{:,n_R} = [\mathbf{F}_{\text{ZFBF}}]_{:,n_R} / \|\mathbf{F}_{\text{ZFBF}}\|_2$, for $n_R = 1, \dots, N_R$, and MBF by using $\mathbf{F}_{\text{MBF}} = \mathbf{H}^H$ and \mathbf{W}_{MBF} such that $[\mathbf{W}_{\text{MBF}}]_{:,n_R} = [\mathbf{F}_{\text{MBF}}]_{:,n_R} / \|\mathbf{F}_{\text{MBF}}\|_2$, for $n_R = 1, \dots, N_R$. When a MiLAC is used to perform R-ZFBF, ZFBF, and MBF, we have two choices. First, the MiLAC can be reconfigured to implement an arbitrary beamforming matrix, as discussed in Section IV-A. Thus, its tunable admittance components can be set according to (20) and (21), where \mathbf{W} is the desired beamforming matrix $\mathbf{W}_{\text{R-ZFBF}}$, \mathbf{W}_{ZFBF} , or \mathbf{W}_{MBF} with uniform power allocation, which is digitally computed. Second, the MiLAC can directly compute the precoding matrices of these LMMSE-inspired beamforming techniques in the analog domain, as explained in Section IV-B. In this case, the columns of $\mathbf{W}_{\text{R-ZFBF}}$, \mathbf{W}_{ZFBF} , and \mathbf{W}_{MBF} cannot be individually normalized, and the resulting precoding matrices are given by $\mathbf{W}_{\text{R-ZFBF}} = \sqrt{N_R} \mathbf{F}_{\text{R-ZFBF}} / \|\mathbf{F}_{\text{R-ZFBF}}\|_F$, $\mathbf{W}_{\text{ZFBF}} = \sqrt{N_R} \mathbf{F}_{\text{ZFBF}} / \|\mathbf{F}_{\text{ZFBF}}\|_F$, and $\mathbf{W}_{\text{MBF}} = \sqrt{N_R} \mathbf{F}_{\text{MBF}} / \|\mathbf{F}_{\text{MBF}}\|_F$, where the normalization factor has been included to ensure that the transmit power is the same as with digital beamforming.

In Fig. 5, we report the sum rate versus the SNR P_T / σ_n^2 achieved by digital and MiLAC-aided beamforming, where $N_T = N_R = 4$ and the channels are independent and identically distributed (i.i.d.) Rayleigh distributed with unit path gain. We observe that R-ZFBF is the best precoder, which boils down to ZFBF at high SNR and to MBF at low SNR, for both digital and MiLAC-aided beamforming, as expected from MIMO theory [44, Chapter 12]. MiLAC-aided beamforming

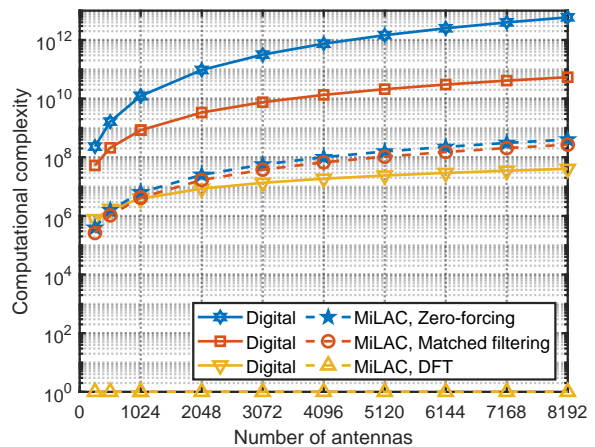


Fig. 7. Computational complexity per coherence block with length $\tau = 100$ symbols of digital beamforming and MiLAC-aided beamforming

performs exactly as digital beamforming when the MiLAC is reconfigured based on the arbitrary beamforming matrix computed digitally, denoted as **MiLAC (arbit.)** in Fig. 5. Besides, MiLAC-aided beamforming suffers a slight performance degradation at high SNR when the LMMSE-inspired beamforming matrix is computed in the analog domain, referred to as **MiLAC (LMMSE)** in Fig. 5. This occurs because, in this case, MiLAC-aided beamforming cannot perform uniform power allocation, which is optimal at high SNR. At the cost of this slight performance degradation, computing the LMMSE-inspired beamforming matrices in the analog domain substantially reduces the required computational complexity, as it will be analyzed in the following.

To compare MiLAC-aided beamforming and digital beamforming at the receiver, we consider a single-user MIMO system with an N_T -antenna transmitter and an N_R -antenna receiver, where the receiver combines the received signal through MMSE, ZF, or MF, as introduced in Section IV-C. In this case, the LMMSE-inspired combining matrices \mathbf{G}_{MMSE} , \mathbf{G}_{ZF} , and \mathbf{G}_{MF} defined in Section IV-C for MiLAC-aided beamforming are also the optimal expressions of the MMSE, ZF, and MF receivers realized with digital beamforming.

In Fig. 6, we report the BER versus the SNR P_T / σ_n^2 obtained with digital and MiLAC-aided beamforming with $N_T = N_R = 4$ and QPSK modulation. Since MiLAC-aided beamforming can implement the same combining matrices as digital beamforming, the two beamforming strategies achieve exactly the same BER.

B. Computational Complexity Evaluation

To quantify the benefits of MiLAC-aided beamforming in terms of computational complexity, we consider a MIMO system with N_T transmitting antennas and N_R receiving antennas, with $N_T = N_R$, where MiLAC-aided beamforming is used at the transmitter to perform R-ZFBF, ZFBF, and MBF, at the receiver for MMSE, ZF, and MF, and for DFT, as discussed in Section IV-B, IV-C, and IV-D. In the considered system, the beamforming matrix is reconfigured per coherence block, where each coherence block includes τ symbol

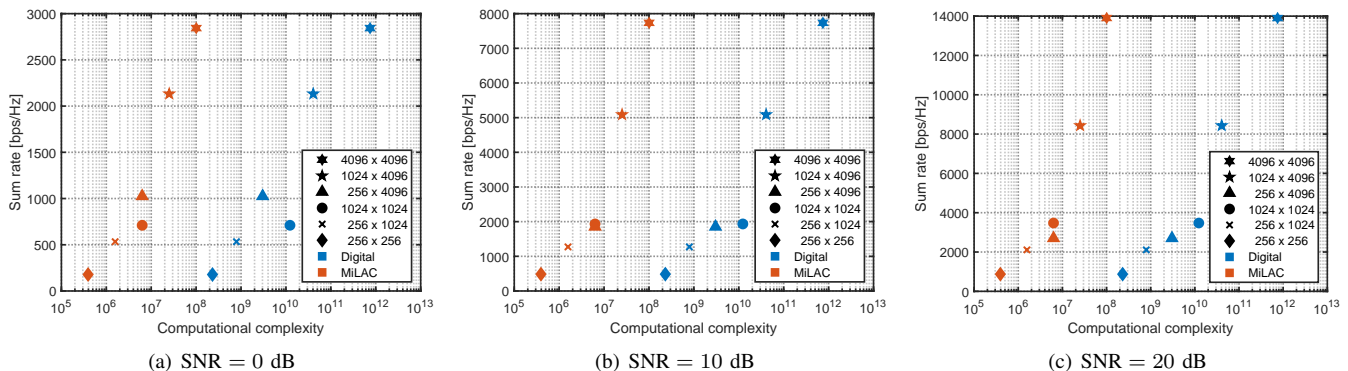


Fig. 8. Sum rate versus computational complexity of R-ZFBF performed in a $N_R \times N_T$ system with digital and MiLAC-aided beamforming, for three different levels of SNR. Markers in blue correspond to digital beamforming and in red to MiLAC-aided beamforming.

transmissions. We define the computational complexity as the number of real operations per coherence block, as analyzed in the following.

- **Zero-forcing.** For R-ZFBF and ZFBF at the transmitter, or MMSE and ZF at the receiver, MiLAC-aided beamforming requires $6N_R^2$ operations per coherence block, as specified in Remarks 2 and 3, and no operation is required on a per-symbol basis. Conversely, with digital beamforming, these strategies require $8(N_R^3 + N_R^3/3)$ operations to design the beamforming matrix at each coherence block (see Remarks 2 and 3). In addition, a matrix-vector product ($\mathbf{W}\mathbf{s}$ or $\mathbf{G}\mathbf{y}$) is performed on a per-symbol basis, requiring $8N_R^2$ real operations per symbol time and making the complexity per coherence block of digital beamforming $8(N_R^3 + N_R^3/3) + 8N_R^2\tau$.
- **Matched filtering.** For MBF at the transmitter, or MF at the receiver, MiLAC-aided beamforming requires $4N_R^2$ operations per coherence block, as given in Remarks 2 and 3, with no operation on a per-symbol basis. Besides, performing these strategies with digital beamforming requires $8N_R^2$ real operations per symbol time to perform the matrix-vector product $\mathbf{W}\mathbf{s}$ or $\mathbf{G}\mathbf{y}$, while no computation is needed to design the beamforming matrix, making the complexity per coherence block $8N_R^2\tau$.
- **DFT.** Performing the DFT with MiLAC-aided beamforming requires no operation, since the MiLAC is not reconfigured at run-time (see Remark 4). Conversely, computing digitally the DFT requires $34/9N_R \log_2(N_R)$ operations per symbol time [46], giving $34/9N_R \log_2(N_R)\tau$ operations per coherence block.

In Fig. 7, we show the computational complexity of digital and MiLAC-aided beamforming, as a function of the number of antennas $N_T = N_R$, by fixing $\tau = 100$ symbols per coherence block. For the cases **zero-forcing** and **matched filtering**, MiLAC-aided beamforming demonstrates up to 1.5×10^4 and 2.0×10^2 times lower computational complexity compared to digital beamforming, respectively, when the number of antennas is $N_R = 8192$. This significant reduction comes because of two reasons. First, MiLAC-aided beamforming does not require the computation of the product $\mathbf{W}\mathbf{s}$, or $\mathbf{G}\mathbf{y}$, on a per-symbol basis, which has significant complexity given the high value of τ [4]. Second, for **zero-forcing**, the

complexity of MiLAC-aided beamforming scales with $\mathcal{O}(N_R^2)$ instead of $\mathcal{O}(N_R^3)$ since the expensive computation of the beamforming matrix is not required. Besides, in the case of **DFT**, MiLAC-aided beamforming does not require any computation, saving up to 4.0×10^7 operations per coherence block when $N_R = 8192$. Given this significant reduction in computational complexity, we expect a proportional reduction in central processing unit (CPU) energy consumption and processing time.

C. Relationship Between Performance and Computational Complexity

We have shown that MiLAC-aided beamforming can achieve the same performance as digital beamforming in Figs. 5 and 6, and we have quantified its gain in terms of computational complexity in Fig. 7. We now investigate how the achieved performance and the required computational complexity are related in digital and MiLAC-aided beamforming. To this end, we consider multi-user MISO system with an N_T -antenna transmitter serving N_R single-antenna receivers through R-ZFBF. For digital beamforming, we consider the R-ZFBF beamforming matrix to have uniform power allocation, as in Section VI-A. For MiLAC-aided beamforming, we consider the LMMSE-inspired design discussed in Section IV-B, where the computation of the R-ZFBF beamforming matrix is done in the analog domain.

In Fig. 8, we report the achieved sum rate and required computational complexity for MiLAC-aided and digital R-ZFBF beamforming in the case of different values of N_R and N_T , where $N_R, N_T \in \{256, 1024, 4096\}$ and $N_R \leq N_T$, and SNR, where $\text{SNR} \in \{0, 10, 20\}$ dB. We make the following three observations. First, the sum rate increases with the number of transmit antennas N_T , the number of receivers N_R , and the SNR, for both MiLAC-aided and digital beamforming. Besides, the computational complexity increases with the number of transmit antennas N_T and receivers N_R , for both MiLAC-aided and digital beamforming, while is independent of the SNR. Second, with a high number of transmit antennas, i.e., $N_T \geq 256$, the performance achieved by a MiLAC computing the R-ZFBF matrix in the analog domain as per Section IV-B is the same as with digital beamforming with uniform power allocation. Thus, we can fully exploit the

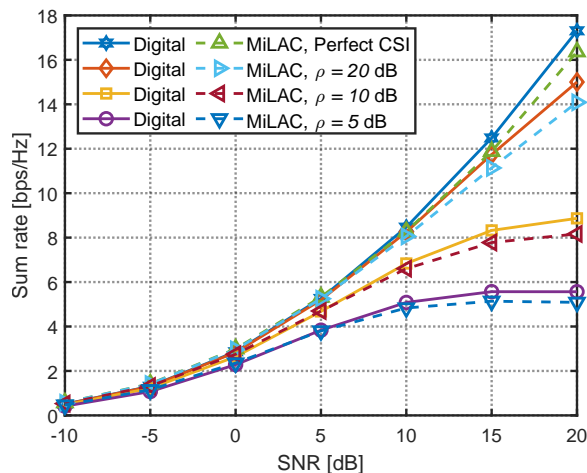


Fig. 9. Sum rate in a 4×4 multi-user MISO system, with noisy CSI.

computational benefits of MiLAC-aided beamforming without sacrificing performance. Third, MiLAC-aided beamforming offers the same performance as digital beamforming for all the considered configurations of N_R , N_T , and SNR, with significant gains in computational complexity. Under a different perspective, MiLAC-aided beamforming can significantly improve the sum rate over digital beamforming given the same computational complexity. For example, MiLAC-aided beamforming can operate R-ZFBF in a system with $N_R = N_T = 4096$ requiring approximately the same complexity as digital R-ZFBF in a system with $N_R = N_T = 256$.

D. Performance Evaluation with Impairments

So far, we have implicitly assumed perfect channel state information (CSI) and that the tunable admittance components of the MiLAC can be reconfigured with arbitrary precision. We now compare MiLAC-aided beamforming with digital beamforming by relaxing these two assumptions, namely in the presence of noisy CSI and discrete-value admittance components in the MiLAC.

Noisy CSI is modeled by adding AWGN to the perfect CSI \mathbf{H} , with different levels of SNR $\rho \in \{20, 10, 5\}$ dB. In Fig. 9, we report the sum rate achieved by R-ZFBF implemented with MiLAC-aided beamforming and digital beamforming optimized based on noisy CSI. For MiLAC-aided beamforming, we consider that the MiLAC is reconfigured to operate LMMSE-inspired beamforming, as explained in Section IV-B. We observe that with $\rho = 20$ dB the performance obtained by MiLAC-aided beamforming and digital beamforming is similar to the performance in the case of perfect CSI. Besides, the performance degrades as ρ decreases. MiLAC-aided beamforming approximately performs as digital beamforming for all the values of ρ , with a slight performance degradation at high SNR, as observed for perfect CSI in Fig. 5.

For practical implementation, it is convenient to design a MiLAC with tunable admittance components whose values are selected from a codebook of limited cardinality. To this end, we notice that the optimal admittance components $Y_{i,k}$ with $i \neq k$ are distributed as the entries of the channel \mathbf{H} when the

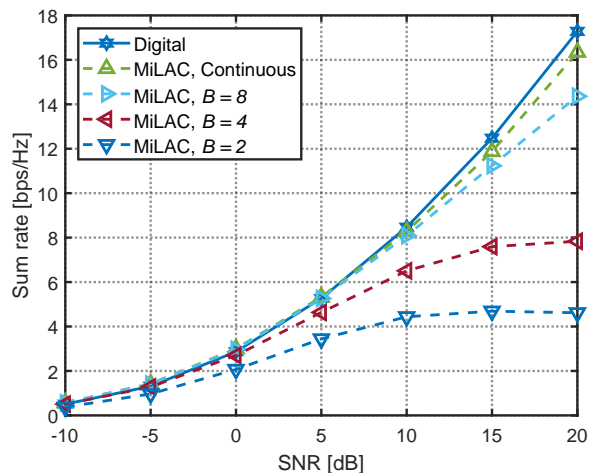


Fig. 10. Sum rate in a 4×4 multi-user MISO system, where the MiLAC has discrete-valued tunable admittance components.

MiLAC is used to perform R-ZFBF, following (8) and Tab. III. Thus, $Y_{i,k}$ with $i \neq k$ have real and imaginary parts Gaussian distributed in the case of i.i.d. Rayleigh fading channels, which can be optimally quantized according to [47]. In Fig. 10, we report the sum rate achieved by R-ZFBF implemented with MiLAC-aided beamforming where the admittance components $Y_{i,k}$ with $i \neq k$ are discretized with B bits of resolution, where $B \in \{8, 4, 2\}$. For the tunable components $Y_{i,k}$ with $i \neq k$, we quantize both their real and imaginary parts with $B/2 \in \{4, 2, 1\}$ bits of resolution according to [47]. In contrast, for the tunable components $Y_{k,k}$, we assume that they can take arbitrary values for simplicity, as they are just $N_T + N_R$. Comparing Figs. 9 and 10, we notice that the impact of discrete-value admittance components with $B \in \{8, 4, 2\}$ resolution bits is similar to the impact of noisy CSI with SNR $\rho \in \{20, 10, 5\}$ dB, respectively. This is because the signal-to-quantization-noise ratio (SQNR) obtained by optimally quantizing a real Gaussian with $B/2 \in \{4, 2, 1\}$ bits is $\rho' \in \{20.2, 9.30, 4.40\}$ dB [47], respectively, which is approximately $\rho \in \{20, 10, 5\}$ dB.

VII. CONCLUSION

In Part II of this paper, we demonstrate the application of MiLAC to wireless communications, highlighting its potential to support communications with thousands of antennas by enabling analog-domain computations and beamforming. We first derive five special cases of the LMMSE estimator that have a practical interest in wireless communications, such as the LS and MF, and illustrate how they can be computed by a MiLAC in the analog domain. Following the capability of a MiLAC to compute such special cases, we introduce MiLAC-aided beamforming as a novel beamforming strategy enabled by a MiLAC. Compared to state-of-the-art beamforming strategies, MiLAC-aided beamforming offers the following five unique benefits in terms of performance, hardware complexity, and computational complexity. First, it has the same flexibility as digital beamforming, allowing us to achieve maximum performance. Second, it requires the minimum number of costly RF chains, i.e., equal to the number

of transmitted symbols. Third, it can be realized with low-resolution ADCs/DACs since the symbols are precoded fully in the analog domain. Fourth, it does not perform any operation on a per-symbol basis, since it does not require precoding in the digital domain. Fifth, it can offer a significant computational complexity reduction in the case of ZF operations at the transmitter or at the receiver, which can be performed with complexity growing with the square of the antenna number, rather than the cube. Numerical results support the theoretical insights, showing that MiLAC-aided beamforming can offer a remarkable reduction in computational complexity. For example, ZF can be achieved with a complexity reduction of 1.5×10^4 times.

Future research directions include modeling MiLAC accounting for hardware non-idealities and its implementation to assess its feasibility and power consumption. It will also be interesting to investigate whether MiLAC architectures with reduced circuit complexity are viable, for example including a reduced number of tunable admittance components. Early contributions in this direction can be found in [48], [49].

REFERENCES

- [1] M. Nerini and B. Clerckx, "Enabling gigantic MIMO beamforming with analog computing," *arXiv preprint arXiv:2504.07477v1*, 2025.
- [2] M. Nerini and B. Clerckx, "Analog computing for signal processing and communications – Part I: Computing with microwave networks," *arXiv preprint arXiv:2504.06790*, 2025.
- [3] E. G. Larsson, O. Edfors, F. Tufvesson, and T. L. Marzetta, "Massive MIMO for next generation wireless systems," *IEEE Commun. Mag.*, vol. 52, no. 2, pp. 186–195, 2014.
- [4] E. Björnson, E. G. Larsson, and T. L. Marzetta, "Massive MIMO: Ten myths and one critical question," *IEEE Commun. Mag.*, vol. 54, no. 2, pp. 114–123, 2016.
- [5] E. Björnson, F. Kara, N. Kolomvakis, A. Kosasih, P. Ramezani, and M. B. Salman, "Enabling 6G performance in the upper mid-band by transitioning from massive to gigantic MIMO," *arXiv preprint arXiv:2407.05630*, 2024.
- [6] S. Sun, T. S. Rappaport, R. W. Heath, A. Nix, and S. Rangan, "MIMO for millimeter-wave wireless communications: Beamforming, spatial multiplexing, or both?" *IEEE Commun. Mag.*, vol. 52, no. 12, pp. 110–121, 2014.
- [7] O. E. Ayach, S. Rajagopal, S. Abu-Surra, Z. Pi, and R. W. Heath, "Spatially sparse precoding in millimeter wave MIMO systems," *IEEE Trans. Wireless Commun.*, vol. 13, no. 3, pp. 1499–1513, 2014.
- [8] F. Sahrabi and W. Yu, "Hybrid digital and analog beamforming design for large-scale antenna arrays," *IEEE J. Sel. Top. Signal Process.*, vol. 10, no. 3, pp. 501–513, 2016.
- [9] A. F. Molisch, V. V. Ratnam, S. Han, Z. Li, S. L. H. Nguyen, L. Li, and K. Haneda, "Hybrid beamforming for massive MIMO: A survey," *IEEE Commun. Mag.*, vol. 55, no. 9, pp. 134–141, 2017.
- [10] I. Ahmed, H. Khammari, A. Shahid, A. Musa, K. S. Kim, E. De Poorter, and I. Moerman, "A survey on hybrid beamforming techniques in 5G: Architecture and system model perspectives," *IEEE Commun. Surv. Tutor.*, vol. 20, no. 4, pp. 3060–3097, 2018.
- [11] T. Gong, N. Shlezinger, S. S. Ioushua, M. Namer, Z. Yang, and Y. C. Eldar, "RF chain reduction for MIMO systems: A hardware prototype," *IEEE Syst. J.*, vol. 14, no. 4, pp. 5296–5307, 2020.
- [12] M. Di Renzo, A. Zappone, M. Debbah, M.-S. Alouini, C. Yuen, J. de Rosny, and S. Tretjakov, "Smart radio environments empowered by reconfigurable intelligent surfaces: How it works, state of research, and the road ahead," *IEEE J. Sel. Areas Commun.*, vol. 38, no. 11, pp. 2450–2525, 2020.
- [13] Q. Wu, S. Zhang, B. Zheng, C. You, and R. Zhang, "Intelligent reflecting surface-aided wireless communications: A tutorial," *IEEE Trans. Commun.*, vol. 69, no. 5, pp. 3313–3351, 2021.
- [14] V. Jamali, A. M. Tulino, G. Fischer, R. R. Müller, and R. Schober, "Intelligent surface-aided transmitter architectures for millimeter-wave ultra massive MIMO systems," *IEEE Open J. Commun. Soc.*, vol. 2, pp. 144–167, 2021.
- [15] C. You, B. Zheng, W. Mei, and R. Zhang, "How to deploy intelligent reflecting surfaces in wireless network: BS-side, user-side, or both sides?" *J. Commun. Inf. Netw.*, vol. 7, no. 1, pp. 1–10, 2022.
- [16] Y. Huang, L. Zhu, and R. Zhang, "Integrating intelligent reflecting surface into base station: Architecture, channel model, and passive reflection design," *IEEE Trans. Commun.*, vol. 71, no. 8, pp. 5005–5020, 2023.
- [17] S. Shen, B. Clerckx, and R. Murch, "Modeling and architecture design of reconfigurable intelligent surfaces using scattering parameter network analysis," *IEEE Trans. Wireless Commun.*, vol. 21, no. 2, pp. 1229–1243, 2022.
- [18] H. Li, S. Shen, and B. Clerckx, "Beyond diagonal reconfigurable intelligent surfaces: From transmitting and reflecting modes to single-, group-, and fully-connected architectures," *IEEE Trans. Wireless Commun.*, vol. 22, no. 4, pp. 2311–2324, 2023.
- [19] M. Nerini, S. Shen, H. Li, and B. Clerckx, "Beyond diagonal reconfigurable intelligent surfaces utilizing graph theory: Modeling, architecture design, and optimization," *IEEE Trans. Wireless Commun.*, vol. 23, no. 8, pp. 9972–9985, 2024.
- [20] A. Mishra, Y. Mao, C. D'Andrea, S. Buzzi, and B. Clerckx, "Transmitter side beyond-diagonal reconfigurable intelligent surface for massive MIMO networks," *IEEE Wireless Commun. Lett.*, vol. 13, no. 2, pp. 352–356, 2024.
- [21] J. An, C. Xu, D. W. K. Ng, G. C. Alexandropoulos, C. Huang, C. Yuen, and L. Hanzo, "Stacked intelligent metasurfaces for efficient holographic MIMO communications in 6G," *IEEE J. Sel. Areas Commun.*, vol. 41, no. 8, pp. 2380–2396, 2023.
- [22] J. An, C. Yuen, C. Xu, H. Li, D. W. K. Ng, M. Di Renzo, M. Debbah, and L. Hanzo, "Stacked intelligent metasurface-aided MIMO transceiver design," *IEEE Wireless Commun.*, vol. 31, no. 4, pp. 123–131, 2024.
- [23] M. Nerini and B. Clerckx, "Physically consistent modeling of stacked intelligent metasurfaces implemented with beyond diagonal RIS," *IEEE Commun. Lett.*, vol. 28, no. 7, pp. 1693–1697, 2024.
- [24] N. Shlezinger, O. Dicker, Y. C. Eldar, I. Yoo, M. F. Imani, and D. R. Smith, "Dynamic metasurface antennas for uplink massive MIMO systems," *IEEE Trans. Commun.*, vol. 67, no. 10, pp. 6829–6843, 2019.
- [25] R. J. Williams, P. Ramírez-Espinosa, J. Yuan, and E. de Carvalho, "Electromagnetic based communication model for dynamic metasurface antennas," *IEEE Trans. Wireless Commun.*, vol. 21, no. 10, pp. 8616–8630, 2022.
- [26] H. Prod'homme, J. Tapie, L. L. Magoarou, and P. del Hougne, "Benefits of mutual coupling in dynamic metasurface antennas for optimizing wireless communications—theory and experimental validation," *arXiv preprint arXiv:2502.15565*, 2025.
- [27] H. Kawakami and T. Ohira, "Electrically steerable passive array radiator (ESPAR) antennas," *IEEE Antennas Propag. Mag.*, vol. 47, no. 2, pp. 43–50, 2005.
- [28] B. Han, V. I. Barousis, C. B. Papadias, A. Kalis, and R. Prasad, "MIMO over ESPAR with 16-QAM modulation," *IEEE Wireless Commun. Lett.*, vol. 2, no. 6, pp. 687–690, 2013.
- [29] C. Zhang, S. Shen, Z. Han, and R. Murch, "Analog beamforming using ESPAR for single-RF precoding systems," *IEEE Trans. Wireless Commun.*, vol. 22, no. 7, pp. 4387–4400, 2023.
- [30] R. R. Müller, M. A. Sedaghat, and G. Fischer, "Load modulated massive MIMO," in *2014 IEEE Global Conference on Signal and Information Processing (GlobalSIP)*. IEEE, 2014, pp. 622–626.
- [31] M. A. Sedaghat, V. I. Barousis, R. R. Müller, and C. B. Papadias, "Load modulated arrays: A low-complexity antenna," *IEEE Commun. Mag.*, vol. 54, no. 3, pp. 46–52, 2016.
- [32] W. Tang, M. Z. Chen, J. Y. Dai, Y. Zeng, X. Zhao, S. Jin, Q. Cheng, and T. J. Cui, "Wireless communications with programmable metasurface: New paradigms, opportunities, and challenges on transceiver design," *IEEE Wireless Commun.*, vol. 27, no. 2, pp. 180–187, 2020.
- [33] W. Tang, J. Y. Dai, M. Z. Chen, K.-K. Wong, X. Li, X. Zhao, S. Jin, Q. Cheng, and T. J. Cui, "MIMO transmission through reconfigurable intelligent surface: System design, analysis, and implementation," *IEEE J. Sel. Areas Commun.*, vol. 38, no. 11, pp. 2683–2699, 2020.
- [34] P. Mannocci, E. Melacarne, and D. Ielmini, "An analogue in-memory ridge regression circuit with application to massive MIMO acceleration," *IEEE J. Emerg. Sel. Top. Circuits Syst.*, vol. 12, no. 4, pp. 952–962, 2022.
- [35] P. Mannocci, E. Melacarne, G. Pedretti, C. Villa, F. Sancandi, U. Spagnolini, and D. Ielmini, "Accelerating massive MIMO in 6G communications by analog in-memory computing circuits," in *2023 IEEE International Symposium on Circuits and Systems (ISCAS)*, 2023.
- [36] C. Wang, G.-J. Ruan, Z.-Z. Yang, X.-J. Yangdong, Y. Li, L. Wu, Y. Ge, Y. Zhao, C. Pan, W. Wei *et al.*, "Parallel in-memory wireless computing," *Nature Electronics*, vol. 6, no. 5, pp. 381–389, 2023.

- [37] Z. R. Omam, A. Bagheri, S. Danesh, S. E. Hosseininejad, O. Yurduseven, G. C. Alexandropoulos, and M. Khalily, "STAR-RIS for simultaneous communications and fourier-based AoA sensing: Design and experimentation," *IEEE Antennas Wireless Propag. Lett.*, 2025.
- [38] A. T. Joy, A. Tishchenko, H. Taghvaei, P. Mursia, V. Sciancalepore, and M. Khalily, "RIS-enabled ISAC in 6G: Exploring the role of wave domain computing," *IEEE Commun. Stand. Mag.*, 2025.
- [39] J. An, C. Yuen, Y. L. Guan, M. Di Renzo, M. Debbah, H. Vincent Poor, and L. Hanzo, "Two-dimensional direction-of-arrival estimation using stacked intelligent metasurfaces," *IEEE J. Sel. Areas Commun.*, vol. 42, no. 10, pp. 2786–2802, 2024.
- [40] M. Goldenbaum, H. Boche, and S. Stańczak, "Harnessing interference for analog function computation in wireless sensor networks," *IEEE Trans. Signal Process.*, vol. 61, no. 20, pp. 4893–4906, 2013.
- [41] G. Zhu and K. Huang, "MIMO over-the-air computation for high-mobility multimodal sensing," *IEEE Internet Things J.*, vol. 6, no. 4, pp. 6089–6103, 2019.
- [42] G. Zhu, J. Xu, K. Huang, and S. Cui, "Over-the-air computing for wireless data aggregation in massive IoT," *IEEE Wireless Commun.*, vol. 28, no. 4, pp. 57–65, 2021.
- [43] K. Yang, T. Jiang, Y. Shi, and Z. Ding, "Federated learning via over-the-air computation," *IEEE Trans. Wireless Commun.*, vol. 19, no. 3, pp. 2022–2035, 2020.
- [44] B. Clerckx and C. Oestges, *MIMO wireless networks: Channels, techniques and standards for multi-antenna, multi-user and multi-cell systems*. Academic Press, 2013.
- [45] C. A. Balanis, *Antenna theory: Analysis and design*. John Wiley & Sons, 2015.
- [46] S. G. Johnson and M. Frigo, "A modified split-radix FFT with fewer arithmetic operations," *IEEE Trans. Signal Process.*, vol. 55, no. 1, pp. 111–119, 2007.
- [47] J. Max, "Quantizing for minimum distortion," *IRE Trans. Inf. Theory*, vol. 6, no. 1, pp. 7–12, 1960.
- [48] M. Nerini and B. Clerckx, "Capacity of MIMO systems aided by microwave linear analog computers (MiLACs)," *arXiv preprint arXiv:2506.05983*, 2025.
- [49] M. Nerini and B. Clerckx, "MIMO systems aided by microwave linear analog computers: Capacity-achieving architectures with reduced circuit complexity," *arXiv preprint arXiv:2506.15052*, 2025.